Baroclinic Interleaving Instability: A Second-Moment Closure Approach

W. D. SMYTH, H. BURCHARD, AND L. UMLAUF

Leibniz Institute for Baltic Sea Research, Warnemünde, Germany

(Manuscript received 5 April 2011, in final form 5 November 2011)

ABSTRACT

Interleaving motions on a wide, baroclinic front are modeled using a second-moment closure to represent unresolved fluxes by turbulence and salt fingering. A linear perturbation analysis reveals two broad classes of unstable modes. First are scale-selective modes comparable with interleaving as observed in oceanic fronts. These correspond well with observations in some respects but grow by a very different mechanism, which ought to be easily distinguished in hydrographic profiles. The second mode type is the so-called ultraviolet catastrophe, which is expected to lead to steppy profiles even in the absence of interleaving. Both modes are driven by positive feedbacks between interleaving and the underlying small-scale mixing processes. Contrary to expectations, use of the second-moment closure in place of earlier empirical mixing models does not lead to improved agreement with observations.

1. Introduction

The original theory of thermohaline interleaving (Stern 1967) identified salt fingers as the driving mechanism. This idea has become widely accepted, especially since the observations of interleaving in Meddy Sharon (MS) (Armi et al. 1989) were explained successfully by that theory (Ruddick 1992). When baroclinicity is accounted for, however, this mechanism becomes highly sensitive to smoothing by mechanically driven turbulence (Zhurbas et al. 1988; Kuzmina and Rodionov 1992; Zhurbas and Oh 2001). Zhurbas and Oh (2001) showed that typical levels of ocean turbulence should damp the instability completely.

Smyth and Ruddick (2010) addressed this paradox by showing that, when the turbulent Prandtl number is much greater than unity (which is true when the Richardson number is high), turbulence not only does not damp the instability as rapidly but can in fact generate its own distinct mode of interleaving instability. Unfortunately, the oceanic implications of these findings remain uncertain because of strong assumptions that underlie the mixing model. Our intention here is to reduce that uncertainty by testing the sensitivity of the Smyth and Ruddick (2010) results to the assumptions made about mixing. To this end, we repeat the stability analysis using a very different parameterization based on the second-moment closure for double-diffusive mixing recently developed by Canuto et al. (2010). Despite the extreme difference in parameterizations, we find once again that turbulence can drive the growth of interleaving instabilities.

The early interleaving theories (Stern 1967; Toole and Georgi 1981; McDougall 1985) assumed that mixing coefficients were constant in space and time. Walsh and Ruddick (1995) allowed the saline diffusivity due to salt fingering to vary with the density ratio R_ρ and found that the effect on growth rates was potentially significant. A more dramatic effect emerged when Walsh and Ruddick (2000) allowed the flux ratio γ to vary, as it does in the linear theory of salt fingering. In addition to the usual scale-selective interleaving mode, a new instability emerged. The growth rate of the new mode was found to increase monotonically with increasing wavenumber, therefore showing no preferred length scale. Walsh and Ruddick (2000) referred to this as "ultraviolet catastrophe" (UVC), in analogy with the original theory of blackbody radiation that grew without bound at short wavelengths. A similar instability has since been invoked by Radko (2003) to explain the formation of thermohaline staircases.

UVC had been seen previously in the work of Phillips (1972), who found this behavior in a simple model of homogeneous, stratified turbulence. The essential assumption was that eddy diffusivity decreased with increasing static stability, so that well-mixed regions would become more turbulent and vice versa, creating a positive feedback loop. Because the process depends entirely on diffusion,

Corresponding author address: W. D. Smyth, College of Oceanic and Atmospheric Sciences, Oregon State University, Corvallis, OR 97331.
E-mail: smyth@coas.oregonstate.edu

DOI: 10.1175/JPO-D-11-066.1

its rate grows quadratically with increasing vertical wavenumber. The aforementioned theories are all linear and therefore become invalid as the disturbances grow to finite amplitude. Posmentier (1977) used a numerical solution of the nonlinear initial value problem to show that the finite-amplitude result of the Phillips UVC was a steplike profile of density.

Smyth and Ruddick (2010) investigated an extended model of interleaving on a baroclinic front, in which a cross-front density gradient was in thermal wind balance with an alongfront current. Once again they found the potential for UVC-type instabilities. They argued that, because only the diffusive terms matter at sufficiently small scale, the other effects that lead to interleaving are irrelevant. UVC can appear on a barotropic front, on a baroclinic front, or in simple homogeneous turbulence as found by Phillips, because it depends only on vertical mixing processes.

All of the aforementioned theories used empirical models for the vertical mixing coefficients. Effective diffusivities representing turbulence and salt fingering were assumed to be either constant or functions of a single parameter: R_ρ for salt fingering and the Richardson number Ri for turbulence. Moreover, the diffusivities were assumed to simply add. Mixing due to turbulence and salt fingering and the interactions between the two processes are in fact much more complex than this (e.g., Wells et al. 2001; Kimura and Smyth 2007; Smyth and Kimura 2011; Kimura et al. 2011). Recent advances in second-moment closure modeling (Canuto et al. 2002, 2008, 2010; Kantha et al. 2011) now allow more sophisticated and potentially more realistic parameterizations of these processes. In particular, the recent works of the Canuto group are the first to combine double-diffusive mixing processes with shear-driven turbulence. We therefore have the opportunity to explore interleaving instabilities for the first time in the context of a second-moment closure.

UVC-type instabilities were found in linearized second-order closure models of stratified turbulence such as the Mellor–Yamada level-2.5 model (Mellor and Yamada 1982) by Burchard and Deleersnijder (2001) and Deleersnijder et al. (2008), but in those studies the instabilities were interpreted as shortcomings in the turbulence models. An alternative view is that the UVC modes represent physically real phenomena. This view is supported by numerous observations of layered structures in the ocean (e.g., Gregg 1976; Schmitt et al. 1987).

Smyth and Ruddick (2010) found instabilities based on flux convergence mechanisms similar to the Phillips UVC mode but exhibiting a well-defined vertical scale comparable with observed interleaving. The oceanographic significance of the new modes was unclear because of the unjustified assumption that salt fingering and turbulent diffusivities simply add. Here, we use a second-moment closure model involving very different assumptions; in particular, the additivity assumption is not made. We find both UVC and scale-selective interleaving related to the mode found by Smyth and Ruddick (2010). The latter is driven, however, by a different mechanism.

Like most models of interleaving to date, our approach is based on linearized perturbation theory. This choice complicates observational comparisons, because the early growth phase it describes is rarely discernible in the data. It represents an essential first step, though, because it tells us the length and time scales that must be resolved in any solution of the nonlinear initial value problem. Also, the linearized equations facilitate identification of the feedbacks that drive growth, allowing us to understand the instabilities mechanistically.

We begin in section 2 by developing the perturbation theory based on equations of motion for the resolved currents and buoyancy fields in combination with the k–ϵ equations for unresolved motions. A simplified theory for the UVC modes is derived, and mechanisms of both interleaving and UVC instabilities are described using budgets for perturbation enstrophy and other relevant measures of instability. In section 3, we show explicit results for parameter regimes based on oceanic observations and compare with measured mode properties. Two mode classes are discussed. The first is scale-selective modes comparable with interleaving, though the physics is different, and the second is UVC. Our conclusions are summarized in section 4.

2. Theory

The objective is to describe mixing in a baroclinic frontal zone in the thermocline. Rather than employ empirical models for the vertical mixing as has been done before, we adapt a second-moment closure model based on the k–ϵ formalism (Umlauf and Burchard 2005). The mathematical model for interleaving on a wide, turbulent, baroclinic front has been described previously (e.g., Smyth 2008; Smyth and Ruddick 2010); in section 2a, we give a brief review of the derivation before introducing the new mixing model.

The initial flow consists of a front in which the cross-front buoyancy gradient is in thermal wind balance with the vertical shear of the alongfront current. Major flow elements are imagined to exist in three ranges of physical scales. The largest scale represents the front. Next, we seek instabilities that describe interleaving on vertical scales of 10–100 m in accordance with observations (e.g., Ruddick 1992). Finally, we have small-scale mixing processes, a mixture of salt fingering and shear-driven turbulence with length scales between a few millimeters and a few meters. The latter motions are not resolved

explicitly, but their effects are parameterized via effective diffusivities. Linearization results in a set of six equations in two independent variables: time and the vertical coordinate. These are removed by assuming a normal mode form for the solution, leaving an algebraic eigenvalue problem.

a. The basic equations

Space is measured by the Cartesian coordinates x, y, and z and the corresponding unit vectors $\hat{\mathbf{e}}_x$, $\hat{\mathbf{e}}_y$, and $\hat{\mathbf{e}}_z$, denoting the cross-front, alongfront, and vertical directions, respectively. Motions are taken to be small in lateral scale compared with the width of the front and hence with respect to the earth's radius, so that both the Coriolis parameter f and the background gradients of buoyancy and velocity are constant in time and space.

The fluid is incompressible and Boussinesq. The buoyancy is defined by $b = -g(\rho - \rho_0)/\rho_0$, where ρ is the density with characteristic value ρ_0 and g is the acceleration due to gravity. The equation of state is assumed to be linear, so that b is just the sum of thermal and saline contributions,

$$b = b_T + b_S, \tag{1}$$

with positive b_T being warm and positive b_S being fresh.

The resulting equations of motion are

$$\nabla \cdot \mathbf{v} = 0, \tag{2}$$

$$\frac{D\mathbf{v}}{Dt} = -f\hat{\mathbf{e}}_z \times \mathbf{v} - \nabla p + b\hat{\mathbf{e}}_z + \nu\nabla^2\mathbf{v} + \frac{\partial}{\partial z}\left(K_m\frac{\partial \mathbf{v}}{\partial z}\right), \tag{3}$$

$$\frac{Db_T}{Dt} = \kappa_T\nabla^2 b_T + \frac{\partial}{\partial z}\left(K_T\frac{\partial b_T}{\partial z}\right), \quad \text{and} \tag{4}$$

$$\frac{Db_S}{Dt} = \kappa_S\nabla^2 b_S + \frac{\partial}{\partial z}\left(K_S\frac{\partial b_S}{\partial z}\right), \tag{5}$$

in which $\mathbf{v}$ is the velocity vector with components (u, v, w),

$$\frac{D}{Dt} = \frac{\partial}{\partial t} + \mathbf{v}\cdot\nabla \tag{6}$$

is the material derivative, t is the time, and p is the pressure scaled by ρ_0. Molecular viscosity is ν, and the thermal and saline molecular diffusivities are κ_T and κ_S, respectively.

The final terms of (3)–(5) represent parameterized vertical mixing processes (horizontal mixing is neglected). In previous studies, the associated mixing parameters were taken to be constants or simple functions of background stratification and shear (e.g., Stern 1967; Toole and Georgi 1981; McDougall 1985; Walsh and Ruddick 1995; May and Kelley 1997; Walsh and Ruddick 2000; Smyth and Ruddick 2010). In the present work, unresolved mixing is described using a stratified k–ϵ model (e.g., Umlauf and Burchard 2005), where diffusivities have the general form

$$K_\alpha = 2\frac{k^2}{\epsilon}S_\alpha. \tag{7}$$

The subscript α stands for m, T, or S. The factor $2k^2/\epsilon$ is a diffusivity scale derived from the kinetic energy k' and kinetic energy dissipation rate ϵ of the unresolved motions. This in itself is an important step, because previous mixing models (e.g., Smyth and Ruddick 2010) were functions only of dimensionless parameters and therefore needed an empirical diffusivity scale whose value was unlikely to be universal. Dependence of the parameterized diffusivities on the mean shear and the thermal and saline stratification is introduced via the structure functions $S_\alpha(\mathrm{Ri}, R_\rho, G_m)$ as defined by Canuto et al. (2010, section 4.1).[1] The gradient Richardson number is

$$\mathrm{Ri} = \frac{\partial b/\partial z}{(\partial u/\partial z)^2 + (\partial v/\partial z)^2}, \tag{8}$$

the buoyancy ratio is

$$R_\rho = -\frac{\partial b_T/\partial z}{\partial b_S/\partial z}, \tag{9}$$

and the squared nondimensional time scale is

$$G_m = 4(k^2/\epsilon^2)\Sigma^2, \tag{10}$$

where

$$\Sigma^2 = \left(\frac{\partial u_i}{\partial x_j} + \frac{\partial u_j}{\partial x_i}\right)\frac{\partial u_i}{\partial x_j}, \tag{11}$$

with $i = 1$, 2, or 3 representing u, v, or w, respectively, and $j = 1$, 2, or 3 representing x, y, or z, respectively. Summation over repeated indices is implied.

The evolution equations for k and ϵ are

$$\frac{Dk}{Dt} = \frac{\partial}{\partial z}\left(K_m\frac{\partial k}{\partial z}\right) + P_m + P_b - \epsilon \quad \text{and} \tag{12}$$

$$\frac{D\epsilon}{Dt} = \frac{1}{\sigma_\epsilon}\frac{\partial}{\partial z}\left(K_m\frac{\partial \epsilon}{\partial z}\right) + \frac{\epsilon}{k}(c_1P_m + c_3P_b - c_2\epsilon), \tag{13}$$

where the production terms are $P_m = K_m\Sigma^2$ and $P_b = -K_T\partial b_T/\partial z - K_S\partial b_S/\partial z$ and $\sigma_\epsilon = 1.3$, $c_1 = 1.44$, and

[1] There should be no confusion between the structure function S_α and the subscript S. For example, S_S represents the salinity structure function.

$c_2 = 1.92$ (e.g., Umlauf and Burchard 2005). The remaining ''constant'' c_3 will be discussed in section 2c. The model is now defined by (2)–(5), (12), and (13), together with the auxiliary relations (1) and (7) and closures for the structure functions S_α. For the present study, we use the structure functions described by Canuto et al. (2010). Note that the mixing model describes only the effects of local shear and stratification; nonlocal effects such as the remote generation of internal waves are not included.

b. Flow decomposition

We wish to test the stability of a wide baroclinic front to perturbations having the form of planar intrusions. Intrusions are assumed to tilt at a slope ϕ across the front but to have no variation in the alongfront (y) direction. Intrusions with this orientation are generally the most unstable because they are not decorrelated by the alongfront shear (Smyth 2008). The buoyancy fields are therefore given by

$$b_\alpha = B_{\alpha x}x + B_{\alpha z}z + b'_\alpha(x,z,t), \tag{14}$$

in which α denotes either S or T. Throughout this paper, the subscripts x, z, and t represent partial derivatives. The background buoyancy gradients $B_{\alpha x}$ and $B_{\alpha z}$ are constants. The prime denotes the perturbation. Similarly, the alongfront velocity is

$$v = V_z z + v'(x,z,t), \tag{15}$$

where the background velocity gradient V_z is a constant. Flow in the x–z plane, being independent of y, is described by a scalar vorticity

$$\omega' = \frac{\partial u'}{\partial z} - \frac{\partial w'}{\partial x}. \tag{16}$$

The turbulence quantities k and ϵ describe a background state of stationary, homogeneous turbulence plus a perturbation,

$$k = \overline{k} + k' \quad \text{and} \tag{17}$$

$$\epsilon = \overline{\epsilon} + \epsilon', \tag{18}$$

where $\overline{k}$ and $\overline{\epsilon}$ are constants. It follows that the diffusivities can be expanded in the same way,

$$K_\alpha = \overline{K}_\alpha + K'_\alpha. \tag{19}$$

We remind the reader that k, ϵ, and K_α are statistical quantities that represent mixing on small scales (centimeters to meters) but that themselves vary only on the scales of interleaving (10–100 m) as represented by the perturbations k', ϵ', and K'_α.

c. Equilibrium states

When all perturbations in (14)–(19) are neglected and the remaining background states are substituted into (2)–(5), the results describe the baroclinic front in steady state. Geostrophic and hydrostatic balances combine to give the thermal wind balance for the alongfront shear,

$$fV_z = B_x = B_{Tx} + B_{Sx}. \tag{20}$$

The vertical buoyancy gradients B_{Tz} and B_{Sz} are uniform, and we assume further that the net stratification is stable,

$$B_z = B_{Tz} + B_{Sz} > 0. \tag{21}$$

In this paper, we focus on the fingering-favorable case $B_{Tz} > 0$; $B_{Sz} < 0$.

It is useful to define the background isohaline, isothermal, and isopycnal slopes as $\phi_S = -B_{Sx}/B_{Sz}$, $\phi_T = -B_{Tx}/B_{Tz}$, and $\phi_\rho = -B_x/B_z$, respectively. Previous studies of the linearized interleaving problem (e.g., May and Kelley 1997) have shown that layers with slope ϕ can be driven by baroclinicity when $0 < \phi < \phi_\rho$ or $\phi_\rho < \phi < 0$. Similarly, layers can be driven by salt fingering when $0 < \phi < \phi_S$ or $\phi_S < \phi < 0$. We also define the equilibrium Richardson number and buoyancy ratio, $\overline{\mathrm{Ri}} = B_z/V_z^2$ and $\overline{R}_\rho = -B_{Tz}/B_{Sz}$. The model we describe here applies to either the fingering-favorable case $\overline{R}_\rho > 1$ or the diffusive convection case $\overline{R}_\rho < 1$, though the latter is beyond the scope of the present investigation.

For stationary, homogeneous turbulence (12) and (13) become

$$P_m + P_b - \epsilon = 0 \quad \text{and} \tag{22}$$

$$c_1 P_m + c_3 P_b - c_2 \epsilon = 0. \tag{23}$$

The structure functions S_α depend not only on Ri and R_ρ but also on G_m. Substituting (7) and (10) in (22), we obtain the nondimensional kinetic energy balance

$$\frac{G_m}{2}(S_m - S_\rho \mathrm{Ri}) = 1, \tag{24}$$

where $S_\rho = (R_\rho S_T - S_S)/(R_\rho - 1)$. Because the mean state is assumed to be stationary, we can obtain G_m as a root of a cubic as described in appendix B of Canuto et al. (2010). The smallest positive root is chosen, because it is continuous with the unstratified solution.

The Canuto et al. (2010) structure functions (Fig. 1) divide the R_ρ–Ri plane roughly into three regions. (The

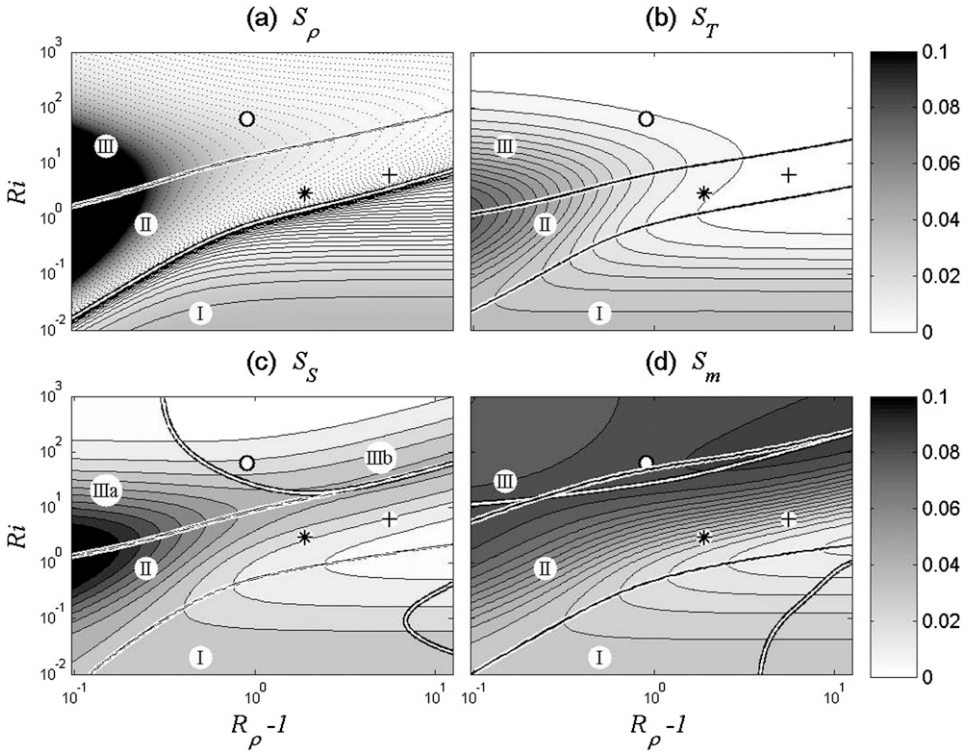

FIG. 1. Structure functions for the Canuto et al. (2010) closure vs density ratio R_ρ and Richardson number Ri: (a) mass, (b) heat, (c) salt, and (d) momentum. Dashed contours show negative values. Circles and asterisks indicate the Richardson numbers for the MS (May and Kelley 2002) and Faroe Front (Hallock 1985) cases, respectively (Table 1). Crosses indicate the maximum scaled growth rate in Fig. 2. Black-on-white curves indicate $\partial S_\alpha/\partial \mathrm{Ri} = 0$. White-on-black curves show (a) $S_\rho = 0$ and (b)–(d) $\partial S_\alpha/\partial R_\rho = 0$. Roman numerals identify the main regions in which the derivatives with respect to R_ρ and Ri are positive or negative.

division is approximate because the extrema of the structure functions lie on slightly different curves.) At low Ri (region I), mixing is dominated by shear-driven turbulence. Values are determined mainly by Ri and decrease as Ri increases. All structure functions are equal to 0.339 in the limit of strong shear, Ri $\to$ 0.

In region II, both salt fingering and turbulence are important. The mass diffusivity K_ρ (or equivalently S_ρ) is negative. All structure functions increase in magnitude with increasing Ri. The increase is especially pronounced in the case of momentum, where it persists to high Ri. Though counterintuitive, these increases are not without support. Recent laboratory experiments (Fernandes and Krishnamurti 2010) and direct simulations (Kimura et al. 2011; Smyth and Kimura 2011) have revealed that weak shear damps finger fluxes, and the relaxation of that damping effect as Ri increases leads to higher diffusivities. Quantitative comparison is difficult because the factor k^2/ϵ was not computed in those experiments.

At high Ri (region III), salt fingering dominates. All scalar diffusivities approach zero as Ri increases, but the eddy viscosity structure function S_m continues to increase up to Ri $\sim 10^2$. Moreover, S_m decreases only slowly at higher Ri in contrast with the other structure functions. The dominance of S_m at high Ri conflicts with predictions of linear theory (Smyth and Kimura 2007) and recent direct simulations (Kimura and Smyth 2007; Kimura et al. 2011; Smyth and Kimura 2011) showing $K_m \ll K_S$ in sheared salt fingers. [This result was first predicted by Ruddick (1985) on the basis of lateral molecular transports.] The difference may exist because the closure model mimics the transition from turbulence to (locally generated) internal waves, in which momentum is transported but not heat or salt. That effect would not be expected in the simulations. The structure functions generally decrease with increasing R_ρ. The exception is the saline structure function S_S, which decreases initially through region IIIa, reaches a minimum when R_ρ is of order unity (depending on Ri), and then increases in region IIIb.

In the perturbation theory developed below, putative stationary states such as those shown by the circles and asterisks are perturbed, causing fluctuations in R_ρ and Ri

and hence in the structure functions. The signs of the derivatives of the structure functions with respect to R_ρ and Ri will prove to be crucial in determining stability. Note that our two observed cases lie in opposite regimes in terms of the signs of these derivatives with respect to Ri. In section 2e, we will see how these derivatives influence the physics of UVC modes.

It would be convenient if c_3 could be regarded, like c_1 and c_2, as a universal constant, but such is not the case; indeed, not even the sign of c_3 is universal. Burchard and Baumert (1995) showed that, in the case of shear-driven turbulence in stratified flow, c_3 must be negative. In convectively driven turbulence, on the other hand, it is easily shown that c_3 must be positive (for a recent review, see Umlauf and Burchard 2005). In general, although the buoyancy production term in the kinetic energy equation can take either sign, we should expect that the corresponding term in the dissipation equation will always represent a source of dissipation. Therefore, we must at this stage regard c_3 as an unknown constant to be determined. To assign a value to c_3 for given steady-state values $\mathrm{Ri} = \overline{\mathrm{Ri}}$ and $R_\rho = \overline{R}_\rho$, we eliminate $\bar{\epsilon}$ between (22) and (23) to obtain

$$c_3 = c_2 + (c_2 - c_1)\frac{\overline{S}_m(\overline{\mathrm{Ri}}, \overline{R}_\rho)}{\overline{S}_\rho(\overline{\mathrm{Ri}}, \overline{R}_\rho)}\frac{1}{\overline{\mathrm{Ri}}}. \tag{25}$$

This result generalizes Burchard and Baumert (1995) to the case of compound stratification. Although any pair of values for $\overline{\mathrm{Ri}}, \overline{R}_\rho$ can be substituted into (25), the result is meaningful only for pairs that represent equilibrium states in seawater. That condition can in principle be expressed as a relation between $\overline{\mathrm{Ri}}$ and $\overline{R}_\rho$. For negative R_ρ, stratified turbulence is known to be in equilibrium at a Richardson number close to 1/4 (e.g., Rohr et al. 1988; Shih et al. 2000), but the introduction of double diffusion alters the equilibrium Ri in ways that are as yet unknown. We await further experiments (most likely direct simulations of homogeneous turbulence with double diffusion) that will allow us to refine this assumption. For now, most of our attention will be on Ri–R_ρ pairs that are estimated from observed mean flows and that may therefore be assumed to be not far from equilibrium.

To evaluate the diffusivities via (7), we will need the scale value $2\overline{k}^2/\bar{\epsilon}$, but the k–ϵ equations do not specify $\overline{k}$ and $\bar{\epsilon}$ separately; all we know is their ratio via (10). The problem can be partially resolved by scaling. For example, if we nondimensionalize using $B_z^{-1/2}$ as the time scale and the Ozmidov scale $L_O = \bar{\epsilon}^{1/2}/B_z^{3/4}$ as the length scale, the results are independent of $\bar{\epsilon}$ (and incidentally B_z). To compare with observations, though, we must have values for the scales. Our approach will be to use measured B_z but then to infer a value for $\bar{\epsilon}$ by fitting the computed interleaving wavelength to observations and ask whether the result is reasonable.

d. Solution for the perturbations

The perturbation equations are obtained by substituting the decompositions (section 2b) into the equations of motion and making three simplifying assumptions. First, we neglect products of perturbation quantities. Second, we assume that all perturbation quantities are uniform on planes parallel to the interleaving motions, defined by $y = \text{constant}$ and $dz/dx = \phi$. Finally, we assume that $\phi \ll 1$, so that $1 + \phi^2$ can be replaced by 1. The result is

$$\omega'_t = fs' + \phi g' + \nu\omega'_{zz} + \overline{K}_m\omega'_{zz}, \tag{26}$$

$$s'_t = -f\omega' - V_z\phi\omega' + \nu s'_{zz} + (\overline{K}_m s' + V_z K'_m)_{zz}, \tag{27}$$

$$g'_{Tt} = (\phi_T - \phi)B_{Tz}\omega' + \kappa_T g'_{Tzz} + (\overline{K}_T g'_T + B_{Tz}K'_T)_{zz}, \quad \text{and} \tag{28}$$

$$g'_{St} = (\phi_S - \phi)B_{Sz}\omega' + \kappa_S g'_{Szz} + (\overline{K}_S g'_S + B_{Sz}K'_S)_{zz}, \tag{29}$$

where $s' = \partial v'/\partial z$ is the perturbation alongfront shear, $g'_\alpha = \partial b'_\alpha/\partial z$ are vertical gradients of the perturbation buoyancy components, and $g' = g'_T + g'_S$.

In the above linearization, we assume that perturbations are infinitesimal in the sense that, for example, $|g'_S| \ll |B_{Sz}|$, to justify discarding products of perturbations. Perturbation theory therefore represents only the earliest phase of the life cycle of an instability.

In (27)–(29), the final pair of terms represents parameterized mixing. In each case, the first of these terms describes a downgradient flux, as would exist if the diffusivities were uniform. [In (26), this is the only parameterized mixing term.] The second term describes effects due to the fluctuations of these parameterized diffusivities in space and time. In the Stern theory of fingering-driven interleaving (e.g., Stern 1967; Toole and Georgi 1981; McDougall 1985; May and Kelley 1997), the thermal and saline buoyancy fluxes are related by a proportionality constant γ. That theory is the special case of (26)–(29) with $K'_m = K'_S = 0$ and $K_T = \gamma K_S/R_\rho$.

In addition to (26)–(29), we now have the perturbation k and ϵ equations,

$$k'_t = P'_m + P'_b - \epsilon' + \overline{K}_m k'_{zz} \quad \text{and} \tag{30}$$

$$\epsilon'_t = \frac{\bar{\epsilon}}{\overline{k}}(c_1 P'_m + c_3 P'_b - c_2\epsilon') + \frac{\overline{K}_m}{\sigma_\epsilon}\epsilon'_{zz}. \tag{31}$$

Perturbations to the production terms are given by

$$P'_m = 2\overline{K}_m V_z s' + V_z^2 K'_m \quad \text{and} \tag{32}$$

$$P'_b = -\overline{K}_T g'_T - B_{Tz} K'_T - \overline{K}_S g'_S - B_{Sz} K'_S. \tag{33}$$

Linearizing (7), we express the diffusivity perturbations as

$$K'_\alpha = 2\frac{\overline{k}^2}{\overline{\epsilon}} S'_\alpha + 2\left(\frac{2\overline{k}}{\overline{\epsilon}} k' - \frac{\overline{k}^2}{\overline{\epsilon}^2}\epsilon'\right)\overline{S}_\alpha. \tag{34}$$

As discussed above, the structure functions have the form $S_\alpha(\mathrm{Ri}, R_\rho, G_m)$. Following Canuto et al. (2010), we approximate G_m by its equilibrium value, which satisfies (24) and which is itself a function of Ri and R_ρ. Accordingly, $S_\alpha = S_\alpha(\mathrm{Ri}, R_\rho)$ and perturbations are expanded as

$$\frac{S'_\alpha}{\overline{S}_\alpha} = S_\alpha^{\mathrm{Ri}} \frac{\mathrm{Ri}'}{\overline{\mathrm{Ri}}} + S_\alpha^{R_\rho} \frac{R'_\rho}{\overline{R}_\rho}, \tag{35}$$

where the constants S_α^{Ri} and $S_\alpha^{R_\rho}$ are defined as

$$S_\alpha^{\mathrm{Ri}} = \frac{\mathrm{Ri}}{\overline{S}_\alpha}\frac{\partial S_\alpha}{\partial \mathrm{Ri}}; \quad S_\alpha^{R_\rho} = \frac{R_\rho}{\overline{S}_\alpha}\frac{\partial S_\alpha}{\partial R_\rho} \tag{36}$$

and the fluctuations in the density ratio and the Richardson number are

$$\frac{\mathrm{Ri}'}{\overline{\mathrm{Ri}}} = \frac{g'_S + g'_T}{B_z} - 2\frac{s'}{V_z} \quad \text{and} \tag{37}$$

$$\frac{R'_\rho}{\overline{R}_\rho} = \frac{g'_T}{B_{Tz}} - \frac{g'_S}{B_{Sz}}. \tag{38}$$

Note that (36) can be written in the equivalent form

$$S_\alpha^{\mathrm{Ri}} = \frac{\mathrm{Ri}}{\overline{K}_\alpha}\frac{\partial K_\alpha}{\partial \mathrm{Ri}}; \quad S_\alpha^{R_\rho} = \frac{R_\rho}{\overline{K}_\alpha}\frac{\partial K_\alpha}{\partial R_\rho} \tag{39}$$

using (7). For the present application, the derivatives in (36) are computed numerically to machine precision using fourth-order finite differences.

The perturbations are assumed to have the normal mode form

$$\{\omega', s', g'_T, g'_S, k', \epsilon'\} = e^{im(z-\phi x)+\sigma t}\{\hat{\omega}, \hat{s}, \hat{g}_T, \hat{g}_S, \hat{k}, \hat{\epsilon}\}, \tag{40}$$

where m is the vertical component of the wave vector and ϕ is the interleaving slope. Time dependence is expressed by σ, the exponential growth rate. Real (complex) σ indicates stationary (oscillatory) instability. The constants $\{\hat{\omega}, \ldots\}$ are complex amplitudes. Combining the perturbation Eqs. (26)–(29) with (30), (31), and the relations (32)–(40), we arrive at a matrix eigenvalue problem,

$$\sigma \mathbf{v} = \mathbf{A}\mathbf{v}. \tag{41}$$

The eigenvector $\mathbf{v}$ is $\{\hat{\omega}, \hat{s}, \hat{g}_T, \hat{g}_S, \hat{k}, \hat{\epsilon}\}^{\mathrm{T}}$ and $\mathbf{A}$ is a 6×6, real stability matrix whose elements are given explicitly in the appendix. The interleaving instabilities of interest here generally have real σ, and the corresponding eigenvectors are chosen to be real.

e. Ultraviolet catastrophe

UVC modes are solutions of the eigenvalue problem (41) having growth rates that are positive and proportional to m^2 in the limit $m^2 \to \infty$. To examine this limit, we divide (41) by m^2 and take $1/m^2 \to 0$, effectively eliminating all terms in the stability matrix $\mathbf{A}$ (given in the appendix) that are not proportional to m^2. Three modes with negative definite growth rates can be eliminated immediately, after which (41) becomes

$$\sigma_0 \mathbf{v} = A_0 A_1 \mathbf{v}, \tag{42}$$

where $\sigma_0 = \sigma/m^2$, $\mathbf{v} = \{\hat{s}, \hat{g}_T, \hat{g}_S\}^{\mathrm{T}}$,

$$\mathbf{A}_0 = \frac{2\overline{k}^2}{\overline{\epsilon}}\begin{bmatrix} -\overline{S}_m & 0 & 0 \\ 0 & -\overline{S}_T & 0 \\ 0 & 0 & -\overline{S}_S \end{bmatrix}, \quad \text{and} \tag{43}$$

$$\mathbf{A}_1 = \begin{bmatrix} 1 - 2S_m^{\mathrm{Ri}} & \dfrac{V_z}{B_z}\left(S_m^{\mathrm{Ri}} + \dfrac{R_\rho - 1}{R_\rho} S_m^{R_\rho}\right) & \dfrac{V_z}{B_z}[S_m^{\mathrm{Ri}} - (R_\rho - 1)S_m^{R_\rho}] \\ -2\dfrac{B_z}{V_z}\dfrac{R_\rho}{R_\rho - 1}S_T^{\mathrm{Ri}} & 1 + \dfrac{R_\rho}{R_\rho - 1}S_T^{\mathrm{Ri}} + S_T^{R_\rho} & \dfrac{R_\rho}{R_\rho - 1}S_T^{\mathrm{Ri}} + R_\rho S_T^{R_\rho} \\ 2\dfrac{B_z}{V_z}\dfrac{S_S^{\mathrm{Ri}}}{R_\rho - 1} & -\dfrac{S_S^{\mathrm{Ri}}}{R_\rho - 1} - \dfrac{1}{R_\rho}S_S^{R_\rho} & 1 - \dfrac{S_S^{\mathrm{Ri}}}{R_\rho - 1} - S_S^{R_\rho} \end{bmatrix}. \tag{44}$$

Because $\mathbf{A}_0$ is nonsingular, the condition for marginal instability is

$$||\mathbf{A}_1|| = 0, \tag{45}$$

where double bars indicate the determinant.

The Phillips mode (Phillips 1972; Posmentier 1977; Ruddick et al. 1989) can be recovered from (45) by assuming that stratification is due entirely to salt, so that $R_\rho = 0$, $S_T^{\mathrm{Ri}} = 0$, and all derivatives with respect to R_ρ vanish. The condition for UVC instability becomes

$$2S_m^{\mathrm{Ri}} - S_S^{\mathrm{Ri}} > 1. \tag{46}$$

If we consider only the mixing of salinity, (46) becomes $S_S^{\mathrm{Ri}} < -1$; that is, diffusivity must decrease with increasing Richardson number faster than Ri^{-1}.

Another possibility of interest is that only momentum is mixed, in which case (46) requires that $S_m^{\mathrm{Ri}} > ½$. This is unlikely in pure turbulence but, when salt fingering is included, S_m^{Ri} can in fact be positive (e.g., Fig. 1d, region II), because increasing Ri relaxes the damping effect of shear. We will see an example of this mechanism for UVC creation in section 3.

The finger-driven UVC mode of Walsh and Ruddick (2000) is obtained by assuming that S_m and S_S are constants and that S_T depends only on R_ρ. This reduces (45) to $1 + S_T^{R_\rho} < 0$. Following Walsh and Ruddick (2000), we now define an effective flux ratio γ such that $S_T = \gamma S_s/R_\rho$. This γ is analogous to the flux ratio for salt fingering, but it also includes fluxes due to turbulence. Substituting and using the definition (36), we obtain $d\gamma/dR_\rho < 0$ as the condition for UVC instability. This is equivalent to (34) of Walsh and Ruddick (2000). In the absence of turbulence, this becomes the Radko (2003) mechanism for staircase formation.

The general solution of (42) for the Canuto et al. (2010) model is shown in Fig. 2. We plot σ_0 scaled by $\overline{k}^2/\overline{\epsilon}$ for a range of oceanically relevant Ri and R_ρ. The UVC mode is present whenever Ri exceeds a critical value that depends on R_ρ but is close to unity for the range of R_ρ where salt fingering is observed. The UVC is strongest, in the sense that the growth rate increases most rapidly with wavenumber, when $R_\rho = 6.6$ and Ri = 6.0. The two observed examples (circle and asterisk in Fig. 2) both lie well within the UVC region, and we will see that both parameter sets yield UVC modes.

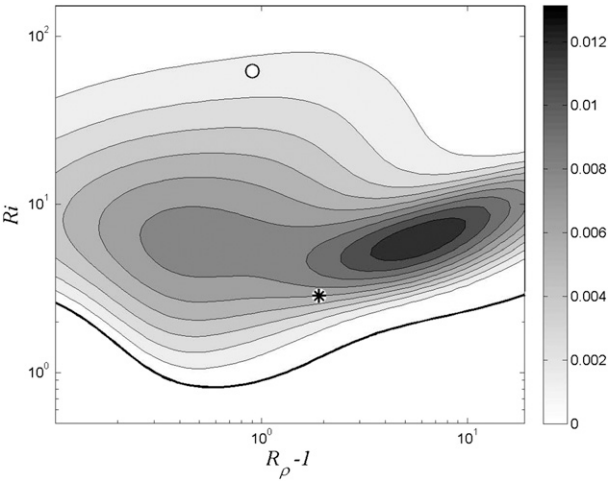

FIG. 2. UVC growth rates for the Canuto et al. (2010) model, obtained as solutions of (42). Equation (45) is satisfied above the thick curve. Shading indicates the growth rate scaled by the wavenumber and the diffusivity scale, $(\sigma/\mu^2)\overline{\epsilon}/\overline{k}^2$. The circle and asterisk indicate MS and Faroe Front parameter values (Table 1).

f. Diagnostic budgets

Besides computing the properties of unstable modes, we wish to understand the physical processes that drive them. The relevant processes will be quantified using budget equations for several perturbation quantities. In section 3, these budgets will be used in the development of intuitively simple conceptual models for the main feedbacks that drive instability in two observed examples, Meddy Sharon and the Faroe Front. Although the budgets given in this section are comprehensive, the most detailed descriptions are reserved for the terms that are most important in those examples.

1) ENSTROPHY

In the classical theory of thermohaline interleaving, the instability can be seen as beginning with the second term on the right-hand side of (26). Here, the buoyancy perturbation g', acting at an angle $\arctan\phi$, drives vorticity ω'. A direct effect of this vorticity is seen in the first term on the right-hand side of (27), where the interleaving motions drive a Coriolis acceleration in the alongfront direction, generating the alongfront shear perturbation s'. Interleaving also advects the alongfront velocity gradient, as shown by the second term on the right-hand side of (27). Both ω' and s' are acted on by various mixing processes. These are generally expected to smooth the vorticity perturbations, but they can sometimes do the reverse. All of these processes will now be quantified in a budget for the perturbation enstrophy $\omega'^2 + s'^2$. The budget has two parts,

$$\omega'\omega'_t = \phi\omega' g' + f\omega' s' + (\nu + \overline{K}_m)\omega'\omega'_{zz} \quad \text{and} \tag{47}$$

$$s's'_t = -fs'\omega' - V_z\phi s'\omega' + (\nu + \overline{K}_m)s's'_{zz} + V_z s' K'_{mzz}. \tag{48}$$

To use this budget in physical space, we would integrate over one wavelength. The equivalent normal mode form is

$$\sigma_r|\hat{\omega}|^2 = \phi(\hat{\omega}^*\hat{g})_r + f(\hat{\omega}^*\hat{s})_r - m^2(\nu + \overline{K}_m)|\hat{\omega}|^2 \quad \text{and} \tag{49}$$

$$\sigma_r|\hat{s}|^2 = -f(\hat{s}^*\hat{\omega})_r - V_z\phi(\hat{s}^*\hat{\omega})_r - m^2(\nu + \overline{K}_m)|\hat{s}|^2 \underline{- m^2V_z(\hat{s}^*\hat{K}_m)_r}, \tag{50}$$

where asterisks represent complex conjugates, and the subscript r indicates the real part. The final (underlined) term of (50) represents fluctuations in the eddy viscosity and is expanded using (34) and (35),

$$\frac{\hat{K}_m}{\overline{K}_m} = \hat{D} + S_m^{\mathrm{Ri}}\frac{\widehat{\mathrm{Ri}}}{\overline{\mathrm{Ri}}} + S_m^{R_\rho}\frac{\hat{R}_\rho}{\overline{R}_\rho}. \tag{51}$$

The first term on the right-hand side represents the relative perturbation of the diffusivity scale $D = 2k^2/\epsilon$,

$$\hat{D} = 2\frac{\hat{k}}{\overline{k}} - \frac{\hat{\epsilon}}{\overline{\epsilon}}, \tag{52}$$

and the second and third terms contain the relative perturbations of Ri and R_ρ,

$$\frac{\widehat{\mathrm{Ri}}}{\overline{\mathrm{Ri}}} = \frac{\hat{g}_S + \hat{g}_T}{B_z} - 2\frac{\hat{s}}{V_z} \quad \text{and} \tag{53}$$

$$\frac{\hat{R}_\rho}{\overline{R}_\rho} = \frac{\hat{g}_T}{B_{Tz}} - \frac{\hat{g}_S}{B_{Sz}}. \tag{54}$$

After substituting (51) into the underlined term of (50) and adding (49), we have the perturbation enstrophy budget,

$$\sigma_r(|\hat{\omega}|^2 + |\hat{s}|^2) = \omega_{\mathrm{Buoy}} + \omega_{\mathrm{Cor}} + \omega_K + s_{\mathrm{Adv}} + s_{\mathrm{Cor}} + s_K + s_{K'D} + s_{K'\mathrm{Ri}} + s_{K'R_\rho}. \tag{55}$$

The first line represents factors governing ω',

- $\omega_{\mathrm{Buoy}} = \phi(\hat{\omega}^*\hat{g})_r$, creation (or destruction) of enstrophy by buoyancy;
- $\omega_{\mathrm{Cor}} = f(\hat{\omega}^*\hat{s})_r$, effect of the Coriolis rotation of s'; and
- $\omega_K = -m^2(\nu + \overline{K}_m)|\hat{\omega}|^2$, destruction by molecular and mean eddy viscosity.

Terms on the second line affect s' independently of eddy viscosity fluctuations,

- $s_{\mathrm{Adv}} = -V_z\phi(\hat{s}^*\hat{\omega})_r$, advection of the thermal wind shear by interleaving motions.
- $s_{\mathrm{Cor}} = -f(\hat{s}^*\hat{\omega})_r = -\omega_{\mathrm{Cor}}$, the Coriolis rotation of ω' (note that the Coriolis terms ω_{Cor} and s_{Cor} cancel, but their values are of interest, so we keep them separate); and
- $s_K = -m^2(\nu + \overline{K}_m)|\hat{s}|^2$, destruction by molecular and background turbulent viscosity.

The effects of eddy viscosity fluctuations on s' [underlined term in (50)] are described on the third line,

- $s_{K'D} = -m^2V_z\overline{K}_m(\hat{s}^*\hat{D})_r$, effect of viscosity fluctuations due to fluctuations in the turbulent diffusivity scale D;
- $s_{K'\mathrm{Ri}} = -m^2V_z\overline{K}_mS_m^{\mathrm{Ri}}[\hat{s}^*(\widehat{\mathrm{Ri}}/\overline{\mathrm{Ri}})]_r$, effect of viscosity fluctuations due to fluctuations in the Richardson number, where individual contributions from $\hat{s}$, $\hat{g}_T$, and $\hat{g}_S$ are obtained by substituting from (53); and
- $s_{K'R_\rho} = -m^2V_z\overline{K}_mS_m^{R_\rho}(\hat{s}^*\hat{R}_\rho/\overline{R}_\rho)_r$, effect of viscosity fluctuations due to fluctuations in the buoyancy ratio, where individual contributions from $\hat{g}_T$ and $\hat{g}_S$ are recovered by substituting from (54).

2) Net buoyancy gradient

Because buoyancy gradient perturbations are expected to be the main driver of interleaving, it will be helpful to see how those perturbations arise. An equation for the net buoyancy gradient perturbation $g' = g'_T + g'_S$ is obtained by adding (28) and (29),

$$g'_t = (\phi_\rho - \phi)B_z\omega' + \kappa_Tg'_{Tzz} + \kappa_Sg'_{Szz} + \overline{K}_Tg'_{Tzz} + \overline{K}_Sg'_{Szz} + B_{Tz}K'_{Tzz} + B_{Sz}K'_{Szz}. \tag{56}$$

Placing this in normal mode form, multiplying by $\hat{g}^*$, and taking the real part gives the buoyancy gradient variance budget

$$\sigma_r|\hat{g}|^2 = (\phi_\rho - \phi)B_z(\hat{g}^*\hat{\omega})_r - m^2[\kappa_T(\hat{g}^*\hat{g}_T)_r + \kappa_S(\hat{g}^*\hat{g}_S)_r] - m^2[\overline{K}_T(\hat{g}^*\hat{g}_T)_r + \overline{K}_S(\hat{g}^*\hat{g}_S)_r] - m^2[B_{Tz}(\hat{g}^*\hat{K}_T)_r + B_{Sz}(\hat{g}^*\hat{K}_S)_r]. \tag{57}$$

The third line contains terms describing the effects of diffusivity fluctuations. We substitute for $\hat{K}_T$ and $\hat{K}_S$ using equations analogous to (51),

$$\frac{\hat{K}_\alpha}{\overline{K}_\alpha} = \hat{D} + S_\alpha^{\mathrm{Ri}}\frac{\widehat{\mathrm{Ri}}}{\overline{\mathrm{Ri}}} + S_\alpha^{R_\rho}\frac{\hat{R}_\rho}{\overline{R}_\rho}, \tag{58}$$

where the subscript α can stand for either T or S. The result is

$$\sigma_r|\hat{g}|^2 = g_{\mathrm{Adv}} + g_{\mathrm{Mol}} + g_K + g_{K'D} + g_{K'\mathrm{Ri}} + g_{K'R_\rho}. \tag{59}$$

The first three terms are independent of diffusivity fluctuations:

- $g_{\mathrm{Adv}} = (\phi_\rho - \phi)B_z(\hat{g}^*\hat{\omega})_r$ is the along-intrusion advection of the mean buoyancy profile. Substituting from the previous definition, $(\hat{g}^*\hat{\omega})_r = \omega_{\mathrm{Buoy}}/\phi$, this can be rewritten as $g_{\mathrm{Adv}} = \omega_{\mathrm{Buoy}}B_z(\phi_\rho - \phi)/\phi$. Therefore, if g_{Adv} is to produce buoyancy variance in the proper phase relationship with vorticity to drive enstrophy growth, the tilt must lie within the baroclinic wedge, $\phi(\phi_\rho - \phi) > 0$. This result can be interpreted as a condition for interleaving to draw upon the potential energy of the density field. When $\overline{\mathrm{Ri}} < 1$, this term produces interleaving in the form of slantwise convection (McIntyre 1970; May and Kelley 1997).
- $g_{\mathrm{Mol}} = -m^2[\kappa_T(\hat{g}^*\hat{g}_T)_r + \kappa_S(\hat{g}^*\hat{g}_S)_r]$ represents molecular effects. This term can drive interleaving on laboratory scales (Ruddick and Kerr 2003) but is negligible in the present context.
- $g_K = -m^2[\overline{K}_T(\hat{g}^*\hat{g}_T)_r + \overline{K}_S(\hat{g}^*\hat{g}_S)_r]$ represents mixing by perturbations acting on the mean diffusivities. This term can be written as

$$g_K = -m^2\overline{K}_S\frac{r_{TS}\overline{\gamma}/\overline{R}_\rho - 1}{r_{TS} - 1}|\hat{g}|^2. \tag{60}$$

Here, we have used the definitions $r_{TS} = -\hat{g}_T/\hat{g}_S$ for the amplitude ratio,

$$\overline{\gamma} = -\frac{\overline{K}_T B_{Tz}}{\overline{K}_S B_{Sz}} \tag{61}$$

for the mean buoyancy flux ratio, and the relation

$$K_\rho = \frac{\overline{R}_\rho K_T - K_S}{\overline{R}_\rho - 1} \tag{62}$$

for the mass diffusivity. Written in the form (60), g_K is negative (i.e., it tends to damp the instability) when $\overline{\gamma} = \overline{R}_\rho$, as is true for stratified turbulence in the limit of high Reynolds number. The term is positive (promoting growth) in two distinct parameter regimes. If $\overline{R}_\rho/\overline{\gamma} > 1$, consistent with mixing by salt fingers, growth requires that $1 < r_{TS} < \overline{R}_\rho/\overline{\gamma}$, so thermal buoyancy perturbations must dominate. Conversely, if $\overline{R}_\rho/\overline{\gamma} < 1$, as is true both in diffusive convection (Turner 1965) and differential diffusion (Gargett 2003; Hebert 1999; Smyth et al. 2005), the amplitude ratio is limited to the range $\overline{R}_\rho/\overline{\gamma} < r_{TS} < 1$: that is, salinity dominates.

The remaining terms [second line of (59)] describe the effects of fluctuations in the eddy diffusivity, which act on the mean buoyancy gradients to cause convergences and divergences in the buoyancy fluxes:

- $g_{K'D} = -m^2(\overline{K}_T B_{Tz} + \overline{K}_S B_{Sz})(\hat{g}^*\hat{D})_r$ is the effect of diffusivity perturbations due to changes in the turbulent diffusivity scale D. Note that the first factor in parentheses is equal to $\overline{K}_\rho B_z$, which is generally negative in double-diffusive cases.
- $g_{K'\mathrm{Ri}} = -m^2(\overline{K}_T B_{Tz} S_T^{\mathrm{Ri}} + \overline{K}_S B_{Sz} S_S^{\mathrm{Ri}})(\hat{g}^*\widehat{\mathrm{Ri}}/\overline{\mathrm{Ri}})_r$ represents diffusivity perturbations due to changes in Ri. Using (39), this term can also be written as $g_{K'\mathrm{Ri}} = -m^2 B_z \partial K_\rho/\partial\mathrm{Ri}(\hat{g}^*\widehat{\mathrm{Ri}}/\overline{\mathrm{Ri}})_r$. The term in $\widehat{\mathrm{Ri}}$ proportional to $\hat{g}$ [see (53)] makes a positive definite contribution if $\partial K_\rho/\partial\mathrm{Ri} < 0$, which is the case at low and moderate Ri (regions I and II in Fig. 1a).
- $g_{K'R_\rho} = -m^2(\overline{K}_T B_{Tz} S_T^{R_\rho} + \overline{K}_S B_{Sz} S_S^{R_\rho})(\hat{g}^*\hat{R}_\rho/\overline{R}_\rho)_r$ represents effects of fluctuations in R_ρ.

3) Component buoyancy gradients

The individual buoyancy components g_T and g_s have variance budgets with the same form as (59), but the definitions are simpler:

- $g^\alpha_{\mathrm{Adv}} = (\phi_\alpha - \phi)B_{\alpha z}(\hat{g}^*_\alpha\hat{\omega})_r$. As above, we can write this as $g^\alpha_{\mathrm{Adv}} = \omega^\alpha_{\mathrm{Buoy}}B_{\alpha z}(\phi_\alpha - \phi)/\phi$. Here, $\omega^\alpha_{\mathrm{Buoy}} = \phi(\hat{\omega}^*\hat{g}_\alpha)_r$ is the part of the buoyancy driving due to the α component.
- $g^\alpha_{\mathrm{Mol}} = -m^2\kappa_\alpha(\hat{g}^*_\alpha\hat{g}_\alpha)_r$ is negative definite and usually small.
- $g^\alpha_K = -m^2\overline{K}_\alpha(\hat{g}^*_\alpha\hat{g}_\alpha)_r$ represents mixing by perturbations acting on the mean diffusivities and is negative definite because $\overline{K}_\alpha > 0$.
- $g^\alpha_{K'D} = -m^2\overline{K}_\alpha B_{\alpha z}(\hat{g}^*_\alpha\hat{D})_r$.
- $g^\alpha_{K'\mathrm{Ri}} = -m^2\overline{K}_\alpha B_{\alpha z}S^{\mathrm{Ri}}_\alpha(\hat{g}^*_\alpha\widehat{\mathrm{Ri}}/\overline{\mathrm{Ri}})_r$. For the case $\alpha = T$, the term proportional to $\hat{g}_T$ [see (53)] makes a positive definite contribution if $\partial K_T/\partial\mathrm{Ri} < 0$. This is true in regions I and III, but not in region II, where the Faroe Front case lies (Fig. 1b). There, however, $\partial K_S/\partial\mathrm{Ri} > 0$ (Fig. 1c), so that for $\alpha = S$ the term proportional to $\hat{g}_S$ makes a positive definite contribution to $g^\alpha_{K'\mathrm{Ri}}$.
- $g^\alpha{}_{K'R_\rho} = -m^2\overline{K}_\alpha B_{\alpha z}S^{R_\rho}_\alpha(\hat{g}^*_\alpha\hat{R}_\rho/\overline{R}_\rho)_r = -m^2 B_{\alpha z}\partial K_\alpha/\partial R_\rho(\hat{g}^*_\alpha\hat{R}_\rho)_r$, where the second equality follows from (39). For the case $\alpha = T$, the term proportional to $\hat{g}_T$ [see (54)] makes a positive definite contribution if $\partial K_T/\partial R_\rho < 0$, which is true throughout Fig. 1b. For $\alpha = S$, the contribution from the term proportional to $\hat{g}_S$ is positive definite if $\partial K_S/\partial R_\rho > 0$. This is true in region IIIb of Fig. 1c, which includes Meddy Sharon (circle).

4) DIFFUSIVITY SCALE

The final budget that we will find useful describes fluctuations in the turbulent diffusivity scale,

$$D' = 2\frac{k'}{\overline{k}} - \frac{\epsilon'}{\overline{\epsilon}}. \tag{63}$$

Combining (30) and (31), we obtain the evolution equation

$$\overline{k}D'_t = 2k'_t - \frac{\overline{k}}{\overline{\epsilon}}\epsilon'_t = (2 - c_1)P'_m + (2 - c_3)P'_b - (2 - c_2)\epsilon' + \overline{K}_m\overline{k}\left(2\frac{k'_{zz}}{\overline{k}} - \frac{1}{\sigma_\epsilon}\frac{\epsilon'_{zz}}{\overline{\epsilon}}\right). \tag{64}$$

Finally, we expand the production terms using (32) and (33) and the structure functions using (35); convert to normal mode form; multiply by the conjugate; and take the real part,

$$\overline{k}\sigma_r|\hat{D}|^2 = D_{\mathrm{Pm}} + D_{\mathrm{Pb}} + D_\epsilon + D_K + D_{K'D} + D_{K'\mathrm{Ri}} + D_{K'R_\rho}, \tag{65}$$

where

- $D_{\mathrm{Pm}} = 2(2 - c_1)V_z\overline{K}_m(\hat{D}^*\hat{s})_r$ is shear production from shear fluctuations working against the mean eddy viscosity;
- $D_{\mathrm{Pb}} = -(2 - c_3)[\overline{K}_T(\hat{D}^*\hat{g}_T)_r + \overline{K}_S(\hat{D}^*\hat{g}_S)_r]$ is buoyancy production from buoyancy fluctuations working against the mean diffusivities (the net effect on D' depends on the sign of $2 - c_3$: if $c_3 < 2$, the effect on k^2 dominates; if $c_3 > 2$, the effect on ϵ dominates);
- $D_\epsilon = -(2 - c_2)(\hat{D}^*\hat{\epsilon})_r$ is dissipation;
- $D_K = -m^2\overline{K}_m\overline{k}\{2[(\hat{D}^*\hat{k})_r/\overline{k}] - (1/\sigma_\epsilon)[(\hat{D}^*\hat{\epsilon})_r/\overline{\epsilon}]\}$ is a viscous term that is close to being negative definite and would be so if σ_ϵ were equal to one (we use $\sigma_\epsilon = 1.3$);
- $D_{K'\mathrm{D}} = (2 - c_2)\overline{\epsilon}|\hat{D}|^2$ is a self-interaction term that is positive definite because $c_2 < 2$. Despite this, the k–ϵ model is inherently stable because of D_ϵ and D_K,
- $D_{K'\mathrm{Ri}} = [(2 - c_1)\overline{K}_m V_z^2 S_m^{\mathrm{Ri}} - (2 - c_3)(\overline{K}_T B_{Tz} S_T^{\mathrm{Ri}} + \overline{K}_S B_{Sz} S_S^{\mathrm{Ri}})](\hat{D}^*\widehat{\mathrm{Ri}})_r$ is the effect of Ri-generated diffusivity fluctuations on the total (shear plus buoyancy) production of D'; and
- $D_{K'R_\rho} = [(2 - c_1)\overline{K}_m V_z^2 S_m^{R_\rho} - (2 - c_3)(\overline{K}_T B_{Tz} S_T^{R_\rho} + \overline{K}_S B_{Sz} S_S^{R_\rho})](\hat{D}^*\hat{R}_\rho)_r$ is the effect of R_ρ-generated viscous fluctuations on the total production of D'.

For graphical presentation, each term on the right-hand side of each of the budgets is divided by the left-hand side, so that the terms sum to unity.

3. Instabilities of oceanic fronts

Here we compare the predictions of the perturbation theory described above with the observed parameters of finite-amplitude interleaving across baroclinic oceanic fronts. As input, the theory requires values for the nondimensional environmental parameters R_ρ, ϕ_s, and ϕ_ρ, and f/N (note that $\mathrm{Ri} = f^2/B_z\phi_\rho^2$). Meddy Sharon was surveyed in detail (Armi et al. 1989) over a 2-yr period, and the needed parameter values have been summarized conveniently by May and Kelley (2002). Those values are listed in the second column of Table 1. The Faroe Front is much more baroclinic than Meddy Sharon. Five transects across the front were reported by Hallock (1985). Reported data included sections of temperature and density for two individual transects as well as the average of all five, and the needed environmental parameters can therefore be estimated. Here we focus on transect 2 (third column of Table 1) (for further details, see Smyth and Ruddick 2010). Measurable interleaving parameters that we can hope to predict using linear theory include

- the vertical scale of interleaving $\lambda = 2\pi/m$;
- the amplitude ratio $r_{TS} = -\hat{g}_T/\hat{g}_S$; and
- the interleaving slope ϕ.

Note that r_{TS} is just the ratio of thermal to saline fluctuation amplitudes expressed in buoyancy units.

Results from linear theory are presented first in nondimensional form as described in section 2c. For comparison with observations, we dimensionalize these results using the observed N but not the observed $\overline{\epsilon}$. Because $\overline{\epsilon}$ is often not well constrained by the observations, particularly not the locally generated part that we model here, we instead identify the value of $\overline{\epsilon}$ needed to match the observed vertical wavelength and compare that value with whatever information is available. In each case, our objective is to develop a simple description of the main feedbacks that drive instability. These simple models are justified quantitatively in terms of the budgets described in section 2f.

We begin with a control case in which the diffusivities are assumed to be uniform. This is consistent with previous studies, although the values of the diffusivities are computed using the new model. We then allow the diffusivities to vary in accordance with the full closure model.

a. Meddy Sharon with uniform diffusivities

We begin with results from the control case in which diffusivities are computed using the Canuto et al. (2010) model, but these diffusivities are assumed not to fluctuate in response to the instability; that is, we set

TABLE 1. Observed parameter values from the lower flank of MS (May and Kelley 2002; Ruddick 1992) and the Faroe Front (Hallock 1985), transect 2.

Parameter	MS	Faroe Front
Ri	61.8	2.86
R_ρ	1.9	2.9
$10^3 \times \phi_s$	27	19.0
$10^3 \times \phi_\rho$	3.6	17.2
f/N	0.0283	0.0291
B_z (s^{-2})	7.4×10^{-6}	2×10^{-5}
λ (m)	25 ±5	25–100
r_{TS}	2 ±1	1.8 ± 0.5
$10^3 \times s$	5.7 ±2.5	Unknown

$K'_m = K'_T = K'_S = 0$. We also neglect molecular terms. In this case, Eqs. (30) and (31) for k' and ϵ' decouple from the system, leaving a highly simplified, 4×4 stability matrix,

$$\mathbf{A} = \begin{pmatrix} -m^2\overline{K}_m & f & \phi & \phi \\ -(\phi V_z + f) & -m^2\overline{K}_m & 0 & 0 \\ (\phi_T - \phi)B_{Tz} & 0 & -m^2\overline{K}_T & \underline{0} \\ (\phi_S - \phi)B_{Sz} & 0 & 0 & -m^2\overline{K}_S \end{pmatrix}. \tag{66}$$

This is equivalent to the model used in previous studies of baroclinic interleaving (Zhurbas et al. 1988; Kuzmina and Rodionov 1992; Kuzmina and Zhurbas 2000; May and Kelley 1997; Zhurbas and Oh 2001), with one important exception. The underlined element expresses the contribution of salinity perturbations to the growth of temperature perturbations. In the classical theory, this term would be nonzero, reflecting Stern's (1967) hypothesis that the heat flux due to salt fingering is proportional to the corresponding salt flux. Here, we refrain from treating salt fingering and turbulence as separate phenomena and instead use a gradient diffusion formalism to express the net mixing. As a result, the heat flux due to salt fingering is combined with that due to turbulence via the diffusivity $\overline{K}_T$.

Results for the MS case (Ruddick 1992) are shown in Fig. 3. There is a well-defined growth rate maximum with slope 0.0069. This value is within the isohaline wedge $\phi(\phi_S - \phi) > 0$, consistent with salt fingering, but outside the isopycnal wedge $\phi(\phi_\rho - \phi) > 0$, inconsistent with baroclinic forcing. The observed slope is well within the range of observations (Table 1, bottom row).

The vertical scale is $152L_O$, where L_O is the previously defined Ozmidov scale. This matches the observed value 25 m if we set the mean dissipation rate associated with local mixing to 5.4×10^{-10} W kg^{-1}. This is a factor of 4 smaller than the observational estimate by Oakey (1988), 2×10^{-9} W kg^{-1}. The difference is reasonable, given

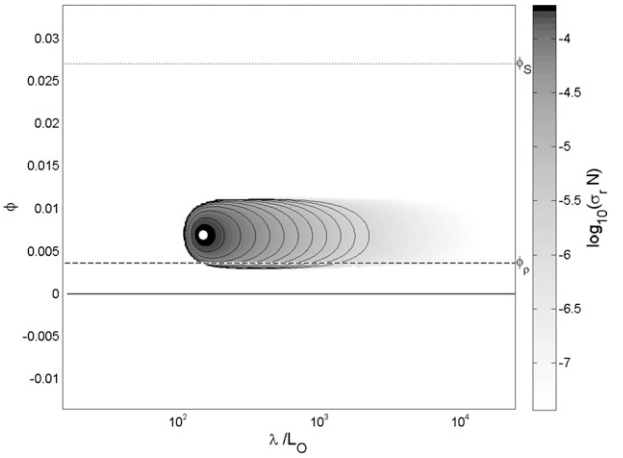

FIG. 3. Nondimensional growth rate vs wavelength–Ozmidov scale and slope for the MS parameters and the constant-diffusivity model. The upper (dotted) and lower (dashed) lines indicate the isohaline and isopycnal slopes, respectively, and the white filled circle indicates the fastest-growing interleaving mode.

that the observed value almost certainly includes a contribution from remotely generated internal waves (which are not represented in the k–ϵ model). Alternatively, we can use the Oakey estimate as our $\overline{\epsilon}$, in which case the predicted vertical scale is 50 m.

The temperature–salinity amplitude ratio is 2.63, indicating that temperature fluctuations are larger (in buoyancy units) than salinity fluctuations. This value is consistent with observations. The maximum growth rate, dimensionalized with the measured buoyancy frequency, is 5.6×10^{-7} s^{-1}. This is roughly consistent with the result obtained by Smyth and Ruddick (2010) using the empirical mixing parameterizations. There it was argued that the growth rate is relatively small because interleaving had already reduced the mean gradients by the time the observations were made.

We look now at the mechanics of the interleaving mode from the constant-diffusivity model. Enstrophy (Fig. 4a) is created in the form of across-front motions driven by buoyancy perturbations. The latter are dominated by temperature (as shown by the annotations T and S), consistent with the fact that $r_{TS} > 1$. The ratio of alongfront to across-front motion is $\hat{s}/\hat{\omega} = -2.5$, indicating a strong effect of Coriolis rotation. Most of the enstrophy is destroyed via dissipation (ω_K and s_K), but a small remainder is stored in the growing perturbation.

The net buoyancy perturbations (Fig. 4b) are created by the mixing term g_K [see discussion in section 2f, especially (60)]. It is not possible to differentiate explicitly between contributions due to salt fingering and turbulence in this model, but the fact that this term is positive for modes with $r_{TS} > 1$ is consistent with salt fingering, as

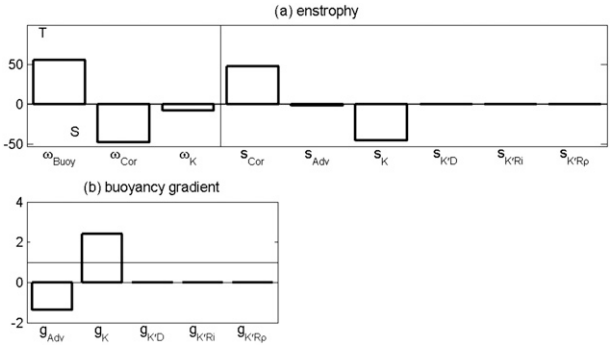

FIG. 4. Budget terms for the MS parameter values, computed using the constant-diffusivity model (66): (a) enstrophy and (b) buoyancy gradient variance. Locations of the annotations T and S indicate thermal and saline contributions to ω_{Buoy}.

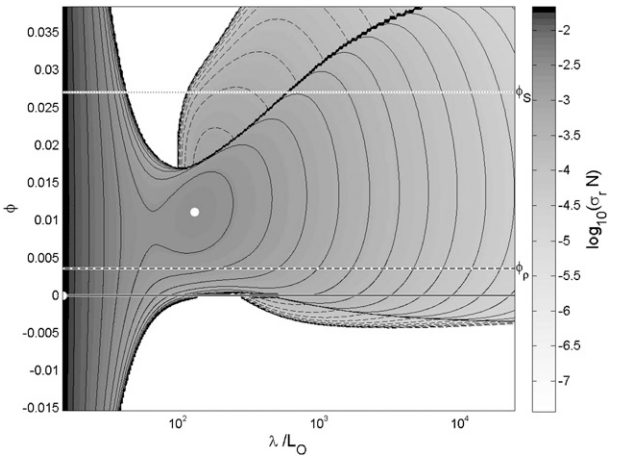

FIG. 5. Nondimensional growth rate vs wavelength–Ozmidov scale and slope for the MS parameters and the full model. Solid (dashed) contours indicate growth rates of stationary (oscillatory) modes. The upper (dotted) and lower (dashed) lines indicate the isohaline and isopycnal slopes, respectively. White filled circles indicate the UVC mode (left edge at $\phi = 0$) and the fastest-growing interleaving mode (local maximum).

is the fact that the modeled structure functions give a flux ratio $\gamma = 0.52$. The buoyancy advection term is negative because the tilt angle lies outside the baroclinic wedge (Fig. 3).

b. Meddy Sharon with the full mixing model

We now recompute the Meddy Sharon case using the full mixing model in which turbulent diffusivities are allowed to fluctuate. The growth rate (Fig. 5) shows a local maximum consistent with interleaving as in the constant-diffusivity case. There are two differences, however. First, for $\lambda/L_O > O(10^2)$ and at sufficiently steep interleaving slopes, the stationary mode bifurcates to become a complex conjugate pair of oscillatory modes. The stationary mode found at lower slopes exhibits the highest growth rate and is therefore of primary interest. Second, small wavelengths (left side of Fig. 5) are dominated by the UVC. In this subsection, we discuss the interleaving mode and the UVC in turn.

1) THE INTERLEAVING MODE

Toward the center of Fig. 5 is a local maximum in the growth rate. This mode has the basic geometry of interleaving, with a well-defined vertical scale. The tilt angle is easily compared with observations. It is between the isopycnal and isohaline slopes as observed and has the numerical value 0.011, somewhat steeper than the observed range 0.0032–0.0082. The growth rate, dimensionalized using the measured $N = 2.72 \times 10^{-3}\ \text{s}^{-1}$, is $8.2 \times 10^{-6}\ \text{s}^{-1}$, which gives an *e*-folding time of 1.4 days. Given that interleaving was observed a matter of a few months after the Meddy's creation, this growth rate is more than sufficient to account for the observations. To match the observed vertical length scale of 25 m, we must dimensionalize using a background dissipation $7.12 \times 10^{-10}\ \text{m}^3\ \text{s}^{-3}$, slightly larger than that needed with the constant-coefficient model (section 3a) but still less than the Oakey (1988) estimate as expected.

An intriguing discrepancy with observations appears when we compute the ratio of the thermal to saline buoyancy fluctuation amplitudes r_{TS}. This ratio is easily computed from observed salinity and temperature profiles. In Meddy Sharon, the ratio was observed to be 2 ± 1. In the present model, we find $r_{TS} = 0.29$. This is not only well outside the range of observations, but it suggests a very different physical mechanism, because the buoyancy fluctuations that drive the computed interleaving mode are dominated by salinity rather than temperature.

One possible explanation is that this is an amplitude effect. Nonlinear simulations (Walsh and Ruddick 1998; Mueller et al. 2007) show that the mixing mechanism acting between layers varies over time as the original buoyancy stratification is amplified and reversed on alternating layer boundaries. If a flow begins in a pure salt fingering regime, it will eventually develop regions of diffusive convection, which promotes $r_{TS} < 1$ [Turner 1965; also section 2f(2) above]. For the mechanism discussed here, the implication is the opposite: layers that start with $r_{TS} < 1$ might transition to a state with $r_{TS} > 1$, as observed in MS, as the mixing mechanisms evolve. Another possibility is that our mixing model is deficient, possibly because the observed values of Ri and R_ρ do not represent an equilibrium state of the k–ϵ equations or because the Canuto et al. (2010) structure functions are not accurate for this parameter regime.

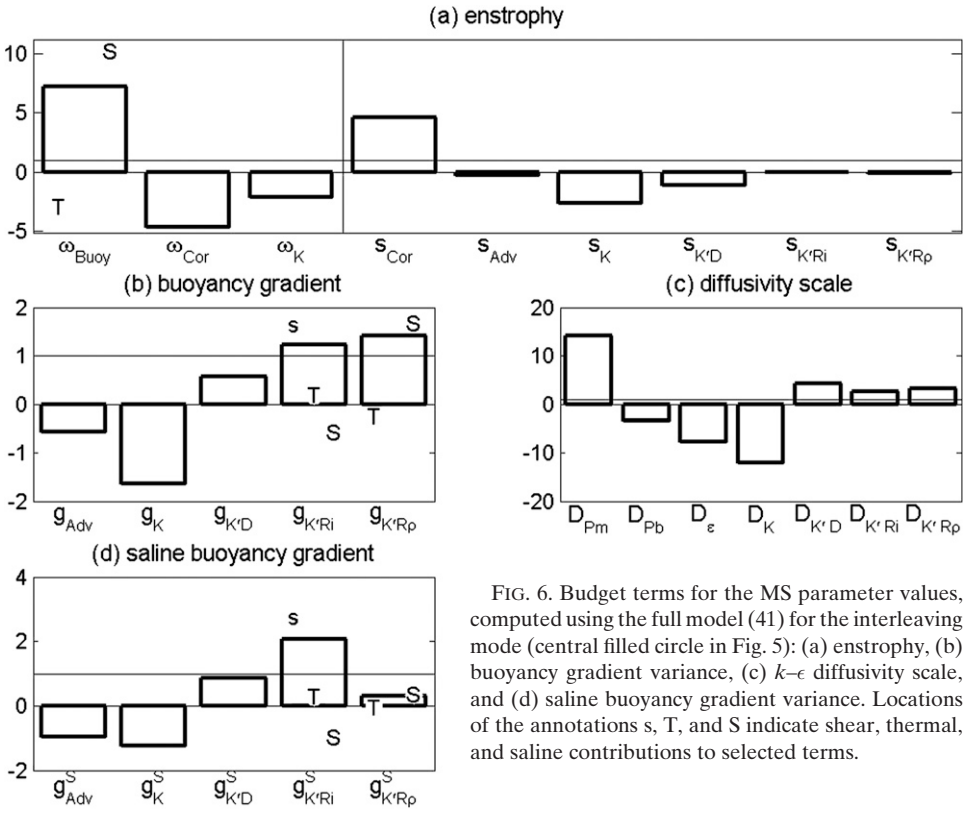

FIG. 6. Budget terms for the MS parameter values, computed using the full model (41) for the interleaving mode (central filled circle in Fig. 5): (a) enstrophy, (b) buoyancy gradient variance, (c) k–ϵ diffusivity scale, and (d) saline buoyancy gradient variance. Locations of the annotations s, T, and S indicate shear, thermal, and saline contributions to selected terms.

To assess the generality of this instability and its dependence on the underlying closure model, we now seek to understand its mechanism. Our approach is to first identify the dominant processes contributing to instability growth and then use that information to extract a simplified model of the mechanism.

As in the constant-diffusivity model, interleaving motions ω' are accelerated by buoyancy fluctuations and then rotated toward the alongfront direction by the Coriolis effect, generating alongfront shear fluctuations (Fig. 6a; cf. Fig. 4a). However, the origin of the buoyancy fluctuations is clearly different (Fig. 6b). The term g_K that created these fluctuations previously is now negative, a result of the fact that r_{TS} is now <1 (see discussion in section 2f). This shows that, in contrast to the constant-diffusivity case, the mean diffusivities associated with salt fingering actually work against the growth of this instability. Instead, this work is done by fluctuations in the diffusivities. Buoyancy gradient fluctuations are created by a mix of three terms associated with scalar diffusivity fluctuations, $g_{K'D}$, $g_{K'\mathrm{Ri}}$, and $g_{K'R_\rho}$. We now discuss these terms in order of size.

- The largest contribution comes via fluctuations in R_ρ, which are driven almost entirely by saline buoyancy. This does not tell us the mechanism of instability, however, unless we also know the origin of the saline buoyancy. That turns out (Fig. 6d) to be generated primarily by fluctuations in Ri driven by the alongfront shear perturbations noted above. We now have a positive feedback loop: from net buoyancy to interleaving vorticity (ω_{Buoy}), via Coriolis to alongfront shear ($\omega_{\mathrm{Cor}} \rightarrow s_{\mathrm{Cor}}$), via Ri and its effect on saline diffusivity to saline buoyancy ($g^S_{K'\mathrm{Ri}}$; shear part), and finally via R_ρ back to net buoyancy ($g_{K'R_\rho}$; salinity part).
- The second-largest contribution to net buoyancy comes more directly via fluctuations in Ri. Because these are driven mainly by the alongfront shear ($g^S_{K'\mathrm{Ri}}$, shear part), we have a second positive feedback loop.
- Finally, net buoyancy is created in part by the term $g_{K'D}$. Through this term, fluctuations in the diffusivity scale $2k^2/\epsilon$ affect the mass diffusivity, driving convergences and divergences in the mass flux. The fluctuations in diffusivity scale are once again the result of the alongfront shear, now acting not through Ri but through the shear production terms in the k–ϵ equations (D_{pm} in Fig. 6c).

In summary, the three positive contributors to the net buoyancy gradient variance can all be understood as originating with the alongfront shear perturbation. Because that shear perturbation is itself generated by the

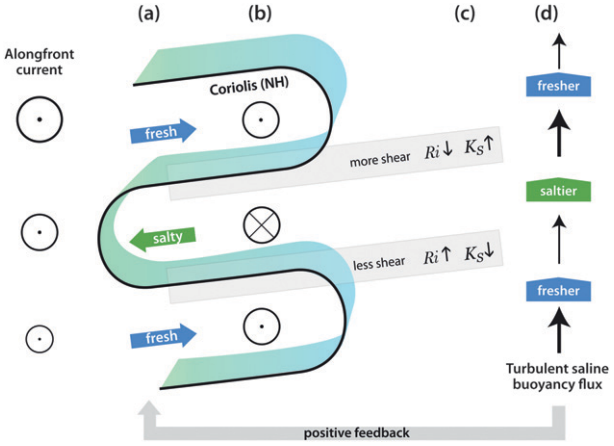

FIG. 7. Simplified mechanics of a turbulence-driven interleaving mode using MS parameter values. (a) Cross-front interleaving motions are driven by saline buoyancy perturbations, and (b) they are then rotated to the alongfront direction by the Coriolis acceleration (Northern Hemisphere is assumed) forming fluctuations in the alongfront current shown by the circular arrows. (c) These lead to fluctuations in the alongfront shear, raising and lowering Ri and thereby altering the saline eddy diffusivity. (d) The upward saline buoyancy flux therefore converges and diverges, and the resulting saline buoyancy perturbations reinforce the original perturbations that drive the interleaving motions in (a). We emphasize that this description represents not a chronological sequence of events but rather a conceptually logical ordering of simultaneous processes.

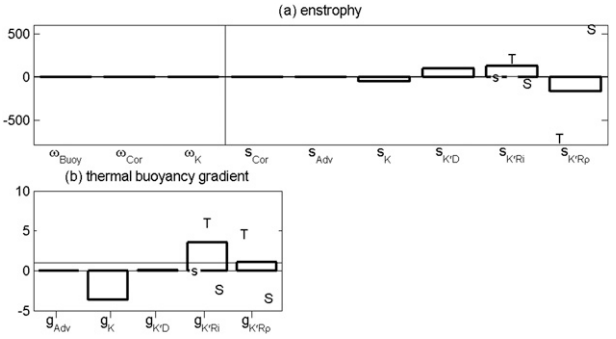

FIG. 8. Budget terms for the MS parameter values, computed using the full model (41) for the UVC mode (filled circle at the left in Fig. 5): (a) enstrophy and (b) thermal buoyancy gradient variance. Locations of the annotations s, T, and S indicate shear, thermal, and saline contributions to selected terms.

net buoyancy gradient (via the Coriolis effect acting on ω'), each process generates a positive feedback loop.

A simpler (though less complete) picture can be conceived if we note that buoyancy fluctuations that drive interleaving are dominantly saline, and therefore focus only on their origin. Saline buoyancy fluctuations are driven primarily by s' via Ri (Fig. 6d, shear contribution to $g^S_{K'\mathrm{Ri}}$). That simpler picture is illustrated schematically in Fig. 7 and explained in the accompanying caption.

We can now understand why the new interleaving mode is salt dominated (i.e., $r_{TS} < 1$). One could imagine the process depicted in Fig. 7, but with temperature taking the place of salinity. The process would still generate positive feedback, but only if the tilt angle were reversed (contrary to the observations), because the turbulent thermal buoyancy flux is directed downward in contrast to the saline buoyancy flux (Fig. 7d). This is essentially the turbulence-generated interleaving mechanism described in section 6f of Smyth and Ruddick (2010), although much lower Ri was required to generate it in that case. The present model does not generate the thermally driven mode because, for a given (absolute) tilt, the flux convergences and divergences would be weaker, because $\partial K_T/\partial\mathrm{Ri}$ is less than $\partial K_S/\partial\mathrm{Ri}$ by a factor of 3 for these parameter values. A given change in Ri therefore results in a larger increase in K_S than in K_T. This difference is compensated partly, but not entirely, by the fact that B_{Tz} is larger (in absolute value) than its saline counterpart by a factor of $R_\rho = 1.9$. In the empirical model of Smyth and Ruddick (2010), only the turbulent component of mixing depends on Ri. For this component $\partial K_T/\partial\mathrm{Ri} = \partial K_S/\partial\mathrm{Ri}$, and the factor R_ρ therefore allows the thermally driven mode to dominate.

2) THE ULTRAVIOLET MODE

Growth rates in the UVC regime (left side of Fig. 5) are nearly independent of the tilt angle. This indicates that the horizontal buoyancy gradients that drive both thermohaline and baroclinic interleaving are irrelevant to the UVC mode in the limit $|m| \to \infty$.

The enstrophy budget (Fig. 8a) reveals significant motions only in the alongfront direction. Unlike interleaving, these motions are driven not by buoyancy but by convergences and divergences in the vertical flux of alongfront momentum due to fluctuations in the effective viscosity K_m. The latter are due mainly to fluctuations in the Richardson number (labeled $s_{\mathrm{K'Ri}}$ in Fig. 8a), which are in turn due mainly to thermal buoyancy fluctuations. (Note that thermal buoyancy plays an opposite role with respect to R_ρ dependence: it overwhelms the positive contribution of saline buoyancy such that the net R_ρ fluctuation is out of phase with the alongfront shear and therefore has a damping effect.) Thermally induced fluctuations in Ri affect turbulent diffusivities in two ways, through the Ri dependence of the structure function and through the turbulent diffusivity scale k^2/ϵ, as we will explain below.

The thermal buoyancy fluctuations are themselves driven by a Phillips–Posmentier mechanism (Figs. 8b, 9a). Thermal fluctuations in the Richardson number cause corresponding fluctuations in the thermal diffusivity, which then act against the background thermal gradient to

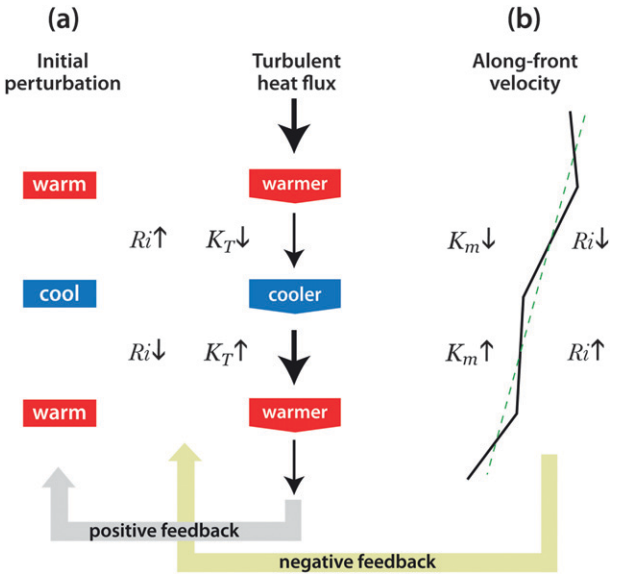

FIG. 9. Mechanics of a UVC mode. (a) Temperature fluctuations are driven by the Phillips mechanism. Initial fluctuations alter the Richardson number, which in turn alters the thermal diffusivity. This causes convergences and divergences in the vertical heat flux, which reinforce the original perturbation. The Ri fluctuations alter K_T in two ways: via the structure function S_m and via the diffusivity scale k^2/ϵ. (b) The Ri fluctuations have the same effect on the eddy viscosity K_m, causing fluctuations in the shear. These feedback negatively on the original Ri fluctuation.

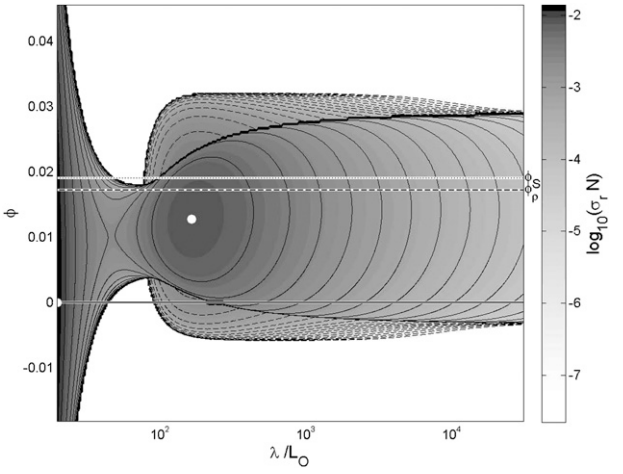

FIG. 10. Nondimensional growth rate vs wavelength–Ozmidov scale and slope for the Faroe Front and the full model. Solid (dashed) contours indicate real (complex) growth rate. The upper (dotted) and lower (dashed) lines indicate the isohaline and isopycnal slopes, respectively, and the white filled circle indicates the fastest-growing interleaving mode.

reinforce the original fluctuations. This is possible in the Meddy Sharon case because $\partial S_T/\partial \mathrm{Ri} < 0$ (Fig. 1b, circle), as discussed in section 2f.

A smaller positive contribution to enstrophy comes from fluctuations in the turbulent viscosity scale $2k^2/\epsilon$ (labeled $s_{K_m'D}$ in Fig. 8a). Like the alongfront motions, these originate from the thermally driven fluctuations in Ri (Fig. 8c). The latter act through the shear and buoyancy production terms to alter k, ϵ, and therefore $2k^2/\epsilon$.

Figure 9a summarizes these processes in schematic form. The fluctuating alongfront shear s' also has a small effect on Ri, but that effect is the wrong sign for growth (Figs. 8a, 9b) because it counters the thermally driven Ri perturbation that drives the instability. The currents associated with this UVC mode are therefore an essentially passive side effect of the Phillips instability.

This UVC mode works with temperature because temperature is stably stratified, and therefore the thermal buoyancy flux is downward. If one substitutes "fresh" and "salty" for "warm" and "cool" in Fig. 9a, one finds that the process does not work; the feedback is negative.

c. *The Faroe Front*

The Faroe Front case differs from Meddy Sharon mainly in that baroclinicity is much stronger, as is reflected in the low Richardson number Ri = 2.86. Once again we see UVC at small scales (Fig. 10, left side). The local growth rate maximum that describes interleaving is within both thermohaline and baroclinic wedges. The dimensional growth rate is large: $\sigma_r = 3.82 \times 10^{-5}$ s^{-1}, equivalent to an e-folding time of only 7.3 h. The observational range for the wavelength is 25–100 m. A fastest-growing mode with wavelength of 25 m is obtained by selecting $\overline{\epsilon} = 1.9 \times 10^{-9}$ W kg^{-1}. The maximum wavelength of 100 m requires $\overline{\epsilon} = 3.1 \times 10^{-8}$ W kg^{-1}. This range of dissipation values is typical of deep ocean observations (Moum and Rippeth 2008). To our knowledge, there are at this time no microstructure observations from the Faroe Front with which to compare directly. The predicted tilt angle is 0.013, and again we have no measurements to compare with. The thermal–saline amplitude ratio r_{TS} is 0.15. As with the Meddy Sharon case, this appears to be at variance with observations: Smyth and Ruddick (2010) inferred a value 1.8 ±0.5 from the measurements of Hallock (1985).

As in the Meddy Sharon case, interleaving motions are driven mainly by the buoyancy term (Fig. 11a). An interesting difference, though, is that the sign of the Coriolis term ω_{Cor} is reversed: the interleaving motions gain enstrophy from the alongfront shear perturbations. The latter must therefore have some other source. We set that question aside for the moment and consider the main source of interleaving, the buoyancy perturbation.

Net buoyancy is created by two processes of similar strength (Fig. 11b).

- The larger is the advection of the background gradient, labeled g_{Adv}. This is consistent with baroclinic

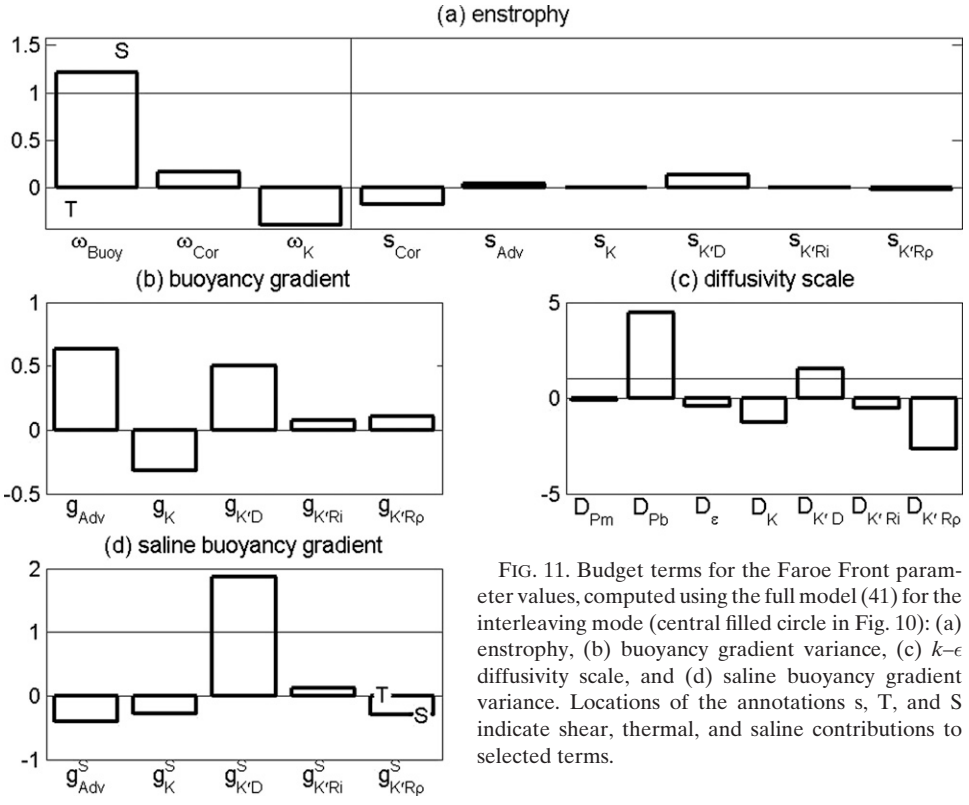

FIG. 11. Budget terms for the Faroe Front parameter values, computed using the full model (41) for the interleaving mode (central filled circle in Fig. 10): (a) enstrophy, (b) buoyancy gradient variance, (c) k–ϵ diffusivity scale, and (d) saline buoyancy gradient variance. Locations of the annotations s, T, and S indicate shear, thermal, and saline contributions to selected terms.

driving, as indicated by the fact that the tilt angle lies within the baroclinic wedge (Fig. 10).

- The second process involves fluctuations in the turbulent diffusivity scale k^2/ϵ. These are driven by salinity fluctuations (Fig. 11d) acting with the mean saline diffusivity via the buoyancy production term (Fig. 11c). This is opposite to the Meddy Sharon interleaving mode, in which diffusivity-scale perturbations were generated by shear perturbations via the shear production term.

Because the first of these is well known (May and Kelley 1997), we focus on the second. The process is illustrated in Figs. 12a–c. Positive saline buoyancy gradient perturbations correspond to enhanced stable stratification. They therefore act through the buoyancy production terms to decrease both k and ϵ. In this case, however, the effect on ϵ is stronger, to the extent that the ratio k^2/ϵ is increased. This strong effect of stable stratification on ϵ results from the fact that $c_3 > 2$, where c_3 is calculated using (25). That constant is unusually large in this case because Ri is unusually small, Ri = 2.86, but still large enough that the net buoyancy flux is dominated by salt fingering. The second term in (25) is therefore relatively large and is positive because $S_\rho < 0$ (Fig. 1d). In response to a reviewer's query, we note that a simplified model in which fluctuations in k^2/ϵ are suppressed does not deliver this interleaving instability; only the UVC is found. In contrast, the interleaving mode found in the MS case [section 3b(1)] changes only slightly when k^2/ϵ is fixed, as one might expect from the fact that the k^2/ϵ budget terms are small (cf. Figs. 6d, 11d).

As noted above, the alongfront shear perturbation does not result from Coriolis turning of interleaving motions as in previous examples. Instead, it is an effect of the fluctuations in k^2/ϵ, which causes convergences and divergences in the vertical flux of alongfront velocity (term labeled $s_{\mathrm{K'D}}$ in Fig. 11a). These are aligned so that, when rotated by the Coriolis acceleration, they reinforce the across-front interleaving motions (terms labeled s_{Cor} and ω_{Cor}) as shown schematically in Fig. 12d.

As in the Meddy Sharon case, the UVC mode (Fig. 13) is essentially a thermally driven Phillips instability, with alongfront shear created passively. A significant difference, though, is that temperature perturbations are created not via Ri but instead via R_ρ. The term $g^T_{K'\mathrm{Ri}}$ that quantifies the Ri effect is now negative because the derivative $\partial K_T/\partial \mathrm{Ri}$ is positive (Fig. 1b).

4. Conclusions

Existing theories of double diffusion at fronts have revealed both realistic interleaving instabilities and

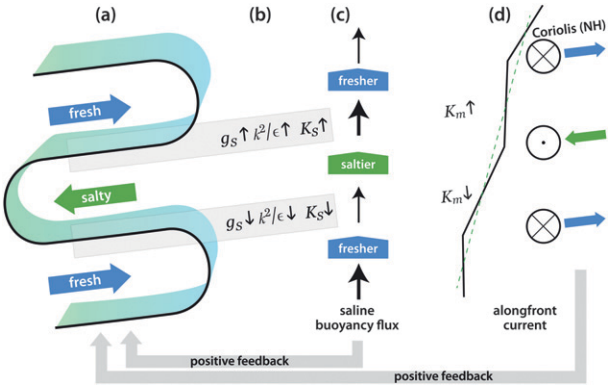

FIG. 12. Interleaving via fluctuations in the effective diffusivities K_s and K_m based on the Faroe Front parameter values. (a) Increased static stability between the fresh upper layer and the salty middle layer (b) damps ϵ more than k^2, increasing k^2/ϵ and hence K_s and vice versa between the middle salty and lower fresh layers. (c) The resulting convergences and divergences in the saline buoyancy flux reinforce the salinity perturbations. (d) Changes in k^2/ϵ also lead to changes in the eddy viscosity K_m and hence in the alongfront shear. The resulting currents are accelerated by planetary rotation to reinforce the original interleaving flow.

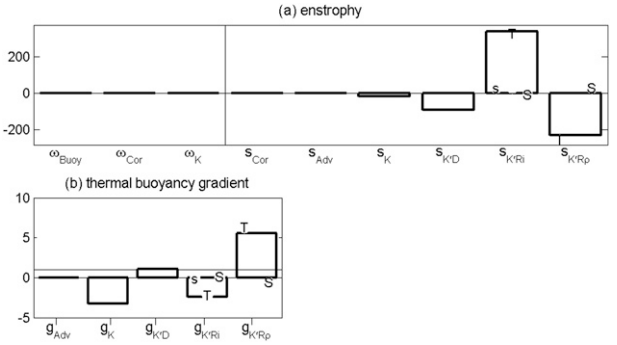

FIG. 13. Budget terms for the Faroe Front parameter values, computed using the full model (41) for the UVC mode (filled circle at the left in Fig. 10): (a) enstrophy and (b) thermal buoyancy gradient variance. Locations of the annotations s, T, and S indicate shear, thermal, and saline contributions to selected terms.

UVC. Here, the empirical mixing models of previous studies are replaced by a state-of-the-art second-moment closure model. The main outcome is that the closure model delivers both interleaving and UVC modes, consistent with the previous results. The mechanism driving the interleaving modes, however, is quite different.

Several areas of uncertainty are worth noting. First, we must keep in mind the limited relevance of linear theory in comparisons with observational data. In deriving (29), for example, we assume that $|g'_S| \ll |B_{Sz}|$. In the Meddy Sharon case, the opposite inequality is true; the fluctuations are sufficient to reverse the background gradient (Armi et al. 1989). This is typical in observed interleaving (Hallock 1985; Grundlingh 1985). Linear theory can excel at predicting finite-amplitude behavior (e.g. salt finger flux ratios; Schmitt 1994; Smyth and Kimura 2007), but it could also do poorly if applied to a system where the mechanism changes at large amplitude. This may be one of the latter cases; Walsh and Ruddick (1998) and Mueller et al. (2007) have shown how the mixing mechanisms that drive interleaving change radically in the nonlinear regime.

Second, although the second-moment model allows us to explore the sensitivity of turbulence effects on interleaving to reasonable assumptions about the nature of the turbulence, it remains open to further development. The ϵ equation (13) has not previously been tested in the presence of double diffusion. The results are sensitive to the value of c_3, which is particularly uncertain. The Canuto et al. (2010) model for the structure functions has been tested with respect to stratified turbulence, but it could evolve as the influence of double diffusion becomes better understood. Finally, we have yet to find a satisfactory way to incorporate mixing due to the breaking of remotely generated internal waves.

With these caveats in mind, we offer the following conclusions:

1) Despite the vastly different approach taken to parameterizing unresolved fluxes, the k–ϵ model with the Canuto et al. (2010) structure functions confirms the Smyth and Ruddick (2010) finding that mechanical turbulence can drive interleaving on a baroclinic front. Like the empirically based parameterization used by Smyth and Ruddick, the k–ϵ model delivers both scale-selective interleaving modes and UVC modes. To capture these processes, inclusion of the effect of the instability upon the parameterized diffusivities is essential.
2) When the k–ϵ model is applied to the Meddy Sharon case, interleaving growth rates and tilt angles are realistic, and the observed vertical scale can be reproduced with a reasonable assumption about the background dissipation rate $\bar{\epsilon}$. These modes are driven by a feedback loop involving salinity; across-front vorticity; and Coriolis-driven alongfront shear, a mechanism that works only if salinity (not temperature) is the dominant perturbation. This last property is contrary to Smyth and Ruddick (2010) and also to observations of finite-amplitude interleaving, which show a dominant temperature signal. This discrepancy with

observations could be an amplitude effect, or it could signal a need for further development of the second-moment closure model in the salt fingering regime.

3) The UVC mode is the Phillips–Posmentier mechanism (Phillips 1972; Posmentier 1977) operating on the thermal buoyancy. Alongfront current fluctuations are created as a passive byproduct of the UVC instability.
4) As in the Meddy Sharon case, the Faroe Front calculations compare reasonably well with observations, except that the intrusions are salinity driven. Because Ri is lower, derivatives of the structure functions with respect to Ri have sign opposite to the Meddy Sharon case (Fig. 1), and the driving mechanism is therefore different. Baroclinic forcing is supplemented by convergences and divergences in the turbulent salt flux driven by fluctuations in the turbulent diffusivity scale k^2/ϵ.
5) The UVC mode is also present in the Faroe Front case and is once again a thermally driven Phillips instability, but the feedback loop works via fluctuations in R_ρ rather than Ri, again because of the different signs of the derivatives of the structure functions with respect to Ri.

This work represents a step beyond thinking of turbulence and double diffusion as separate and independent processes whose diffusivities simply add. The new instability processes are intriguing, though their relevance for the ocean is difficult to assess at present, because observations of frontal interleaving in its early stages are not yet available. Simulations including nonlinear effects [as were done by Walsh and Ruddick (1998) and Mueller et al. (2007) using empirical mixing schemes] will produce results more directly comparable with existing observations.

Current observations represent only a small sampling of the parameter range where interleaving is possible. Recent theoretical work (including the present paper) has shown that interleaving can be generated in myriad ways beyond the original salt fingering mechanism and that the properties of such interleaving may vary widely. This expands the range of what Shcherbina et al. (2009) have called active interleaving mechanisms and may cause some interleaving regimes that have previously been considered passive to be reinterpreted. We hope that these possibilities will inspire future observations of mixing processes in fronts.

Acknowledgments. We appreciate helpful advice from V. Canuto, A. Howard, and Y. Cheng. WDS was supported by the U.S. National Science Foundation under Grant OCE0622922 and by a visiting scholarship from the Leibniz Institute for Baltic Sea Research, Warnemünde, Germany. We thank Dave Reinert for assistance with graphics.

APPENDIX

The Stability Matrix

The elements of the stability matrix are computed as follows: Expansions for the parameterized diffusivity perturbations are obtained by substituting (35)–(38) into (34),

$$\frac{K'_\alpha}{\overline{K}_\alpha} = F_{\alpha s}s' + F_{\alpha T}g'_T + F_{\alpha s}g'_S + F_{\alpha k}k' + F_{\alpha\epsilon}\epsilon', \tag{A1}$$

where

$$F_{\alpha s} = -2\frac{S^{\mathrm{Ri}}_\alpha}{V_z}; \quad F_{\alpha T} = \frac{S^{\mathrm{Ri}}_\alpha}{B_z} + \frac{S^{R_\rho}_\alpha}{B_{Tz}}; \quad F_{\alpha S} = \frac{S^{\mathrm{Ri}}_\alpha}{B_z} - \frac{S^{R_\rho}_\alpha}{B_{Sz}};$$
$$F_{\alpha k} = \frac{2}{\overline{k}}; \quad F_{\alpha E} = -\frac{1}{\overline{\epsilon}}.$$

The stability matrix is expressed in the mnemonic form

$$\mathbf{A} = \begin{pmatrix} A_{\omega\omega} & A_{\omega s} & A_{\omega T} & A_{\omega S} & A_{\omega k} & A_{\omega\epsilon} \\ A_{s\omega} & A_{ss} & A_{sT} & A_{sS} & A_{sk} & A_{s\epsilon} \\ A_{T\omega} & A_{Ts} & A_{TT} & A_{TS} & A_{Tk} & A_{T\epsilon} \\ A_{S\omega} & A_{Ss} & A_{ST} & A_{SS} & A_{Sk} & A_{S\epsilon} \\ A_{k\omega} & A_{ks} & A_{kT} & A_{kS} & A_{kk} & A_{k\epsilon} \\ A_{\epsilon\omega} & A_{\epsilon s} & A_{\epsilon T} & A_{\epsilon S} & A_{\epsilon k} & A_{\epsilon\epsilon} \end{pmatrix}$$

and its elements are given by

$$A_{\omega\omega} = -m^2(\nu + \overline{K}_m); \quad A_{\omega s} = f; \quad A_{\omega T} = A_{\omega S} = \phi;$$
$$A_{\omega k} = A_{\omega E} = 0;$$
$$A_{\omega s} = -\phi V_z - f; \quad A_{ss} = -m^2\overline{K}_m V_z F_{ms} - m^2(\nu + \overline{K}_m);$$
$$A_{sT} = -m^2\overline{K}_m V_z F_{mT}; \quad A_{sS} = -m^2\overline{K}_m V_z F_{mS};$$
$$A_{sk} = -m^2\overline{K}_m V_z F_{mk}; \quad A_{s\epsilon} = -m^2\overline{K}_m V_z F_{m\epsilon};$$
$$A_{T\omega} = (\phi_T - \phi)B_{Tz}; \quad A_{Ts} = -m^2\overline{K}_T B_{Tz} F_{Ts};$$
$$A_{TT} = -m^2\overline{K}_T B_{Tz} F_{TT} - m^2(\kappa_T + \overline{K}_T);$$
$$A_{TS} = -m^2\overline{K}_T B_{Tz} F_{TS}; \quad A_{Tk} = -m^2\overline{K}_T B_{Tz} F_{Tk};$$
$$A_{T\epsilon} = -m^2\overline{K}_T B_{Tz} F_{T\epsilon}; \quad A_{S\omega} = (\phi_S - \phi)B_{Sz};$$
$$A_{Ss} = -m^2\overline{K}_S B_{Sz} F_{Ss}; \quad A_{ST} = -m^2\overline{K}_S B_{Sz} F_{ST};$$

$$A_{SS} = -m^2\overline{K}_S B_{Sz} F_{SS} - \mu^2(\kappa_S + \overline{K}_S);$$

$$A_{Sk} = -m^2\overline{K}_S B_{Sz} F_{Sk}; \quad A_{S\epsilon} = -m^2\overline{K}_S B_{Sz} F_{S\epsilon};$$

$$A_{\omega k} = 0;$$

$$A_{ks} = 2\overline{K}_m V_z + \overline{K}_m V_z^2 F_{ms} - \overline{K}_T B_{Tz} F_{Ts} - \overline{K}_S B_{Sz} F_{Ss};$$

$$A_{kT} = -\overline{K}_T + \overline{K}_m V_z^2 F_{mT} - \overline{K}_T B_{Tz} F_{TT} - \overline{K}_S B_{Sz} F_{ST};$$

$$A_{kS} = -\overline{K}_S + \overline{K}_m V_z^2 F_{mS} - \overline{K}_T B_{Tz} F_{TS} - \overline{K}_S B_{Sz} F_{SS};$$

$$A_{kk} = -m^2\overline{K}_m + \overline{K}_m V_z^2 F_{mk} - \overline{K}_T B_{Tz} F_{Tk} - \overline{K}_S B_{Sz} F_{Sk};$$

$$A_{k\epsilon} = -1 + \overline{K}_m V_z^2 F_{m\epsilon} - \overline{K}_T B_{Tz} F_{T\epsilon} - \overline{K}_S B_{Sz} F_{S\epsilon};$$

$$A_{\epsilon\omega} = 0;$$

$$A_{\epsilon s} = \overline{\epsilon}\overline{k}^{-1}(2c_1\overline{K}_m V_z + c_1\overline{K}_m V_z^2 F_{ms} - c_3\overline{K}_T B_{Tz} F_{Ts} - c_3\overline{K}_S B_{Sz} F_{Ss});$$

$$A_{\epsilon T} = \overline{\epsilon}\overline{k}^{-1}(-c_3\overline{K}_T + c_1\overline{K}_m V_z^2 F_{mT} - c_3\overline{K}_T B_{Tz} F_{TT} - c_3\overline{K}_S B_{Sz} F_{ST});$$

$$A_{\epsilon S} = \overline{\epsilon}\overline{k}^{-1}(-c_3\overline{K}_S + c_1\overline{K}_m V_z^2 F_{mS} - c_3\overline{K}_T B_{Tz} F_{TS} - c_3\overline{K}_S B_{Sz} F_{SS});$$

$$A_{\epsilon k} = \overline{\epsilon}\overline{k}^{-1}(c_1\overline{K}_m V_z^2 F_{mk} - c_3\overline{K}_T B_{Tz} F_{Tk} - c_3\overline{K}_S B_{Sz} F_{Sk}); \quad \text{and}$$

$$A_{\epsilon\epsilon} = -m^2\overline{K}_m\sigma_\epsilon^{-1} + \overline{\epsilon}\overline{k}^{-1}(c_1\overline{K}_m V_z^2 F_{m\epsilon} - c_3\overline{K}_T B_{Tz} F_{T\epsilon} - c_3\overline{K}_S B_{Sz} F_{S\epsilon} - c_2).$$

REFERENCES

Armi, L., D. Hebert, N. Oakey, J. Price, P. Richardson, H. Rossby, and B. Ruddick, 1989: Two years in the life of a Mediterranean salt lens. *J. Phys. Oceanogr.,* **19,** 354–370.

Burchard, H., and Z. Baumert, 1995: On the performance of a mixed layer model based on the k-ϵ turbulence closure. *J. Geophys. Res.,* **100,** 8523–8540.

——, and E. Deleersnijder, 2001: Stability of algebraic non-equilibrium second-order closure models. *Ocean Modell.,* **3,** 33–50.

Canuto, V. M., A. Howard, Y. Cheng, and M. S. Dubikov, 2002: Ocean turbulence. Part II: Vertical diffusivities of momentum, heat, mass, salt, and passive scalars. *J. Phys. Oceanogr.,* **32,** 240–264.

——, Y. Cheng, and A. M. Howard, 2008: A new model for double diffusion + turbulence. *Geophys. Res. Lett.,* **35,** L02613, doi:10.1029/2007GL032580.

——, A. M. Howard, Y. Cheng, C. J. Muller, A. Leboissetier, and S. R. Jayne, 2010: Ocean turbulence, III: New GISS vertical mixing scheme. *Ocean Modell.,* **34,** 70–91.

Deleersnijder, E., E. Hanert, H. Burchard, and H. Dijkstra, 2008: On the mathematical stability of stratified flow models with local turbulence closure schemes. *Ocean Dyn.,* **58,** 237–246.

Fernandes, A., and R. Krishnamurti, 2010: Salt finger fluxes in a laminar shear flow. *J. Fluid Mech.,* **658,** 148–165.

Gargett, A., 2003: Differential diffusion: An oceanographic primer. *Prog. Oceanogr.,* **56,** 559–570.

Gregg, M. C., 1976: Microstructure and intrusions in the California Current. *J. Phys. Oceanogr.,* **6,** 528–555.

Grundlingh, M., 1985: Occurrence of Red Sea water in the southwest Indian Ocean. *J. Phys. Oceanogr.,* **15,** 207–212.

Hallock, Z., 1985: Variability of frontal structure in the southern Norwegian Sea. *J. Phys. Oceanogr.,* **15,** 1245–1254.

Hebert, D., 1999: Intrusions: What drives them? *J. Phys. Oceanogr.,* **29,** 1382–1391.

Kantha, L., S. Carneil, and M. Sclavo, 2011: A note on modeling double diffusive mixing in the global ocean. *Ocean Modell.,* **36,** 40–48.

Kimura, S., and W. Smyth, 2007: Direct numerical simulations of salt sheets and turbulence in a double-diffusive shear layer. *Geophys. Res. Lett.,* **34,** L21610, doi:10.1029/2007GL031935.

——, ——, and E. Kunze, 2011: Turbulence in a sheared, salt-fingering-favorable environment: Anisotropy and effective diffusivities. *J. Phys. Oceanogr.,* **36,** 1144–1159.

Kuzmina, N., and V. Rodionov, 1992: Influence of baroclinicity on formation of thermohaline intrusions in ocean frontal zones. *Izv. Acad. Sci. USSR Atmos. Oceanic Phys.,* **28,** 804–810.

——, and V. Zhurbas, 2000: Effects of double diffusion and turbulence on interleaving at baroclinic ocean fronts. *J. Phys. Oceanogr.,* **30,** 3025–3038.

May, B., and D. Kelley, 1997: Effect of baroclinicity on double-diffusive interleaving. *J. Phys. Oceanogr.,* **27,** 1997–2008.

——, and ——, 2002: Contrasting the interleaving in two baroclinic ocean fronts. *Dyn. Atmos. Oceans,* **36,** 23–42.

McDougall, T., 1985: Double-diffusive interleaving. Part I: Linear stability analysis. *J. Phys. Oceanogr.,* **15,** 1532–1541.

McIntyre, M., 1970: Diffusive destabilization of the baroclinic circular vortex. *Geophys. Fluid Dyn.,* **1,** 19–57.

Mellor, G., and T. Yamada, 1982: Development of a turbulence closure model for geophysical fluid problems. *Rev. Geophys. Space Phys.,* **20,** 851–875.

Moum, J. N., and T. P. Rippeth, 2008: Do observations adequately resolve the natural variability of oceanic turbulence? *J. Mar. Syst.,* **77,** 409–417, doi:10.1016/j.jmarsys.2008.10.013.

Mueller, R. D., W. D. Smyth, and B. R. Ruddick, 2007: Shear and convective turbulence in a model of thermohaline intrusions. *J. Phys. Oceanogr.,* **37,** 2534–2549.

Oakey, N., 1988: Estimates of mixing inferred from temperature and velocity microstructure. *Small-Scale Turbulence and Mixing in the Ocean,* J. Nihoul and B. Jamart, Eds., Elsevier, 239–247.

Phillips, O., 1972: Turbulence in a strongly stratified fluid: Is it unstable? *Deep-Sea Res.,* **19,** 79–81.

Posmentier, E., 1977: The generation of salinity finestructure by vertical diffusion. *J. Phys. Oceanogr.,* **7,** 298–300.

Radko, T., 2003: A mechanism for layer formation in a double diffusive fluid. *J. Fluid Mech.,* **497,** 365–380.

Rohr, J., E. Itsweire, K. Helland, and C. Van Atta, 1988: Growth and decay of turbulence in a stably stratified shear flow. *J. Fluid Mech.,* **195,** 77–111.

Ruddick, B., 1985: Momentum transport in thermohaline staircases. *J. Geophys. Res.,* **90,** 895–902.

——, 1992: Intrusive mixing in a Mediterranean salt lens: Intrusion slopes and dynamic mechanisms. *J. Phys. Oceanogr.,* **22,** 1274–1285.

——, and O. Kerr, 2003: Oceanic thermohaline intrusions: Theory. *Prog. Oceanogr.,* **56,** 483–497.

——, T. McDougall, and J. Turner, 1989: The formation of layers in a uniformly stirred density gradient. *Deep-Sea Res.,* **36,** 579–609.

Schmitt, R. W., 1994: Triangular and asymmetric salt fingers. *J. Phys. Oceanogr.,* **24,** 855–860.

——, H. Perkins, J. D. Boyd, and M. C. Stalcup, 1987: C-SALT: An investigation of the thermohaline staircase in the western tropical North Atlantic. *Deep-Sea Res.,* **34,** 1655–1665.

Shcherbina, A. Y., M. C. Gregg, M. H. Alford, and R. R. Harcourt, 2009: Characterizing thermohaline intrusions in the North Pacific subtropical frontal zone. *J. Phys. Oceanogr.,* **39,** 2735–2756.

Shih, L. H., J. R. Koseff, J. H. Ferziger, and C. R. Rehmann, 2000: Scaling and parameterization of stratified homogeneous turbulent shear flow. *J. Fluid Mech.,* **412,** 1–20.

Smyth, W., 2008: Instabilities of a baroclinic, double diffusive frontal zone. *J. Phys. Oceanogr.,* **38,** 840–861.

——, and S. Kimura, 2007: Instability and diapycnal momentum transport in a double-diffusive stratified shear layer. *J. Phys. Oceanogr.,* **37,** 1551–1565.

——, and B. Ruddick, 2010: Effects of ambient turbulence on interleaving at a baroclinic front. *J. Phys. Oceanogr.,* **40,** 685–712.

——, and S. Kimura, 2011: Mixing in a moderately sheared, salt-fingering layer. *J. Phys. Oceanogr.,* **41,** 1364–1384.

——, J. Nash, and J. Moum, 2005: Differential diffusion in breaking Kelvin–Helmholtz billows. *J. Phys. Oceanogr.,* **35,** 1044–1022.

Stern, M., 1967: Lateral mixing of water masses. *Deep-Sea Res.,* **14,** 747–753.

Toole, J., and D. Georgi, 1981: On the dynamics of double diffusively driven intrusions. *Prog. Oceanogr.,* **10,** 123–145.

Turner, J. S., 1965: The coupled turbulent transports of salt and heat across a sharp density interface. *Int. J. Heat Mass Transfer,* **8,** 759–767.

Umlauf, L., and H. Burchard, 2005: Second-order turbulence closure models for geophysical boundary layers: A review of recent work. *Cont. Shelf Res.,* **25,** 795–827.

Walsh, D., and B. Ruddick, 1995: Double diffusive interleaving: The effect of nonconstant diffusivities. *J. Phys. Oceanogr.,* **25,** 348–358.

——, and ——, 1998: Nonlinear equilibration of thermohaline intrusions. *J. Phys. Oceanogr.,* **28,** 1043–1069.

——, and ——, 2000: Double diffusive interleaving in the presence of turbulence: The effect of a nonconstant flux ratio. *J. Phys. Oceanogr.,* **30,** 2231–2245.

Wells, M., R. Griffiths, and J. Turner, 2001: Generation of density fine structure by salt fingers in a spatially periodic shear. *J. Geophys. Res.,* **106,** 7027–7036.

Zhurbas, V., and I. Oh, 2001: Can turbulence suppress double-diffusively driven interleaving completely? *J. Phys. Oceanogr.,* **31,** 2251–2254.

——, N. Kuzmina, and I. Lozovatskiy, 1988: The role of baroclinicity in intrusive layering in the ocean. *Izv. Acad. Sci. USSR Atmos. Oceanic Phys.,* **28,** 34–36.